REPORT DOCUMENTATION PAGE

Form Approved
OMB No. 0704-0188

1. REPORT DATE *(DD-MM-YYYY)* 16-11-2009	2. REPORT TYPE Journal Article	3. DATES COVERED *(From - To)*

4. TITLE AND SUBTITLE

Data Fusion Analysis For Test Validation System

5a. CONTRACT NUMBER

5b. GRANT NUMBER

5c. PROGRAM ELEMENT NUMBER

6. AUTHOR(S)

Mark Hammond
Christian Minor
Susan Rose-Pehrsson

5d. PROJECT NUMBER
CA09DET503G

5e. TASK NUMBER

5f. WORK UNIT NUMBER

7. PERFORMING ORGANIZATION NAME(S) AND ADDRESS(ES)

Navy Research Laboratory, DC
Nova Research, Inc. , Alexandria, VA

8. PERFORMING ORGANIZATION REPORT NUMBER

9. SPONSORING / MONITORING AGENCY NAME(S) AND ADDRESS(ES)

Defense Threat Reduction Agency
8725 John J Kingman Road
Fort Belvoir, VA 22060-6201

10. SPONSOR/MONITOR'S ACRONYM(S)

11. SPONSOR/MONITOR'S REPORT NUMBER(S)

12. DISTRIBUTION / AVAILABILITY STATEMENT

Distribution A / Approved for public release; distribution is unlimited

13. SUPPLEMENTARY NOTES

14. ABSTRACT

A range test validation system (RTVS) is being developed under the sponsorship of the Defense Threat Reduction Agency. The purpose of RTVS is to provide accurate identification and tracking of clouds of chemical agent stimulants and a means for validation point and standoff chemical sensors on a test grid. As part of the RTVS program, the chemical sensing/ Chemometrics Section (Code 6181) of the Naval Research Laboratory has been tasked to develop the data analysis and data fusion methods.

15. SUBJECT TERMS

range test validation system, data fusion, chemical agent detection tests

16. SECURITY CLASSIFICATION OF: Unclassified			17. LIMITATION OF ABSTRACT	18. NUMBER OF PAGES	19a. NAME OF RESPONSIBLE PERSON Bryan Horner
a. REPORT	**b. ABSTRACT**	**c. THIS PAGE**		58	**19b. TELEPHONE NUMBER** *(include area code)* 7037673379

Standard Form 298 (Rev. 8-98)
Prescribed by ANSI Std. Z39.18

DATA FUSION ANALYSIS FOR RANGE TEST VALIDATION SYSTEM

Christian P. Minor

Nova Research, Inc.
Alexandria, VA

Mark H. Hammond
Susan L. Rose-Pehrsson

Chemical Sensing/Chemometrics Section
Navy Technology Center for Safety and Survivability
Naval Research Laboratory

Table of Contents

DATA FUSION ANALYSIS FOR RANGE TEST VALIDATION SYSTEM

EXECUTIVE SUMMARY

A range test validation system (RTVS) is being developed under the sponsorship of the Defense Threat Reduction Agency. The purpose of RTVS is to provide accurate identification and tracking of clouds of chemical agent simulants and a means for validating point and standoff chemical sensors on a test grid. As part of the RTVS program, the Chemical Sensing/Chemometrics Section (Code 6181) of the Naval Research Laboratory has been tasked to develop the data analysis and data fusion methods.

Data for chemical agent simulants were collected from various sensor systems during test chemical releases at Dugway Proving Ground in Utah in September of 2007 and June of 2008. Members of Code 6181 were present for most of the Dugway testing. The chemical clouds released varied in direction, depending on the wind, and in size, depending on the amount of chemical released. Standoff and point detection systems were positioned to monitor a test grid. These included the following RTVS detection systems: twenty-five IMS-based point sensors (LCD) and Airmar weather stations, and five standoff IR imaging spectrometers (AIRIS). The legacy Dugway sensor systems were comprised of several standoff IR cameras (ORION), standoff FTIR sensors (MESH), photo ionization-based point sensors (ppbRAE), and PWIDS weather stations.

Data from these tests was used to complete an analysis of RTVS data fusion. The majority of the results contained herein were presented to the DTRA program sponsor at monthly progress meetings. The conclusions of NRL"s data fusion analysis for RTVS are as follows:

First, environmental factors significantly affected the testing at Dugway Proving Grounds. Winds induced significant variance in the RTVS data. Testing at night when winds were less variable did mitigate wind effects, but an inverted temperature gradient with respect to height may have affected the calibration and sensing capabilities of the standoff sensors. Testing at night increased the effect, as the temperature gradient was positive and less steep during the day. In addition, a large variation in the RTVS data was observed with respect to the dissemination method. Explosive dissemination generated an uneven, globular release of simulant with unpredictable vaporization. Dissemination by stack release produced a more even distribution of vaporized simulant, but was not consistent with the expected chemical threat scenario.

With respect to the sensor systems, the effective calibration and baselines of the LCD point sensors make them a better choice than the Dugway ppbRAE point sensors for inclusion in RTVS. The three-dimensional AIRIS data cube with individual voxels

covering the test grid to a great height is an extremely flexible format for data fusion. The problems observed with the AIRIS tomographic reconstruction should decrease with further computational power. Overall, the AIRIS sensors provided cloud-tracking capabilities that were similar to the Dugway MESH FTIR sensors, but were at three-times better resolution. Cloud tracking with either AIRIS or MESH was a vast improvement over tracking with the ORION IR cameras, which typically lost track of the cloud within two minutes of its dissemination. Although not yet fully implemented, real-time situational awareness is viable from fused LCD and AIRIS data, but the rate as of the 2008 test series was limited to at best one update per minute (i.e., one data cube) with coverage of the entire test grid.

For RTVS data fusion, the coverage areas of the LCD and AIRIS sensors are effectively disparate and do not overlap, which limits the performance gains possible with multisensor data fusion. However, the LCD and AIRIS sensors jointly provide situational awareness in which detections of simulants are clear indications of a tangible chemical threat, and the absence of detections is an accurate all-clear signal for the test grid as a whole. The combined sensors are not able to effectively distinguish local regions of threat from regions of all clear on the test grid when a simulant has been released due to the large distance between the point sensors, the lack of overlap between the point and standoff sensors, and the variances in the data induced by environmental conditions, dissemination methods, and tomographic reconstruction. The presence of significant numbers of false negatives means that a Dempster-Shafer approach is the most effective strategy for RTVS data fusion. Dempster-Shafer treats all types of information as adding to the total situational awareness, but remains flexible when the absence of information is uncertain or not informative for situational awareness. Additionally, a number of strategies for improving the quality of the LCD and AIRIS data are presented. Heuristic methods would be effective for implementing these strategies. Heuristic rules are also likely to be a useful strategy for RTVS data fusion.

1. INTRODUCTION

Under the sponsorship of the Defense Threat Reduction Agency (DTRA), a range test validation system (RTVS) is being developed to track and detect chemical agent simulant clouds on a test grid. The goal of the program is to determine in near real-time the size, location, and concentration distribution of chemical clouds. The RTVS will be used to validate point and standoff sensors. The data generated will help develop advanced warning and quantitative analysis methods for fugitive emissions.

The tracking system for RTVS includes five infrared imaging spectroradiometers (AIRIS) and 25 point sensors (LCD) based on ion mobility spectrometry (IMS). The data from these detection systems and the weather information recorded at the test sites are used to map the chemical clouds onto a common operational picture. The goal is to develop chemical fate and transport models that can be used to assess the performance of detection systems. The fate and transport models for the chemical cloud rely on the fusion of image data, discrete sensor data at specific locations, and auxiliary information about the test site and weather conditions. These different types of data need to be fused to provide a common operational picture that describes the chemical clouds temporally and spatially.

The Chemical Sensing/Chemometrics Section (Code 6181) of the Naval Research Laboratory has much experience with diverse sensor fusion. Under ONR sponsorship, NRL developed a multi-sensory data fusion detection system to detect shipboard damage control events such as fire, flooding, and pipe ruptures. The detection system combined regular and near-infrared video camera, discrete spectral sensors and a microphone with machine vision, pattern recognition, and data fusion algorithms. The detection system detects in real time flaming and smoldering fires, pipe ruptures, gas leaks and flooding events and has a high immunity to false positives. The Naval Research Laboratory also developed a data fusion framework for wide-area assessment of unexploded ordnance (UXO) using diverse data detection methods and intelligent data fusion [1]. In this program, three airborne techniques: magnetometry, LiDAR, and orthophotography were used with auxiliary site data to identify areas that are likely to be contaminated with UXO.

For the RTVS program, data were collected from various sensor systems during test chemical releases at Dugway Proving Ground in Utah [2, 3]. The chemical clouds released varied in direction, depending on the wind, and in size, depending on the amount of chemical released. Standoff and point detection systems were positioned to monitor a test grid. The complete detection system was comprised of five standoff IR imaging spectrometers (AIRIS) and twenty-five point sensors (LCD) collocated with twenty-five weather stations (Airmar). The results are compared to the legacy systems used at Dugway, which were comprised of standoff IR cameras (ORION), standoff FTIR sensors (MESH), point sensors based on photoionization (ppbRAE), and weather stations (PWIDS).

As part of this effort, NRL has used the RTVS test data to develop data analysis and data fusion methods for the test grid. Relevant components of the data fusion framework developed for wide-area assessment of UXO have been adapted for application to RTVS sensing systems and the utility of several feature extraction techniques have been evaluated with sensor data.

The report is structured as follows: Following the Introduction, the standoff and point sensors developed for the RTVS program are briefly described in the Background section, as well as the Dugway sensing systems. Next, strategies for implementing data fusion with multisensor systems are discussed in the Method section. Those strategies with which NRL has had the most success are emphasized. The RTVS testing and evaluation performed in 2007 and 2008 is then described in the Experimental section. The description is limited to that necessary for understanding the three-dimensional nature of the test site and testing conditions, as more information is available in the test summary reports. Next, the Results and Discussion section comprises NRL"s data fusion analysis for the RTVS program. Finally, Conclusions are presented. A summary of the conclusions is also provided in the Executive Summary.

2. BACKGROUND

2.1. Sensor Systems

Two sensing components were developed for use in the RTVS test grid. One of these was a ground-based array of 25 chemical point detectors and weather stations that were dispersed at regular intervals across the grid. The ground-based array was developed by ECBC and referred to as "SPIDAR," short for Spectrometric Point Ionizing Detector ARray.

The chemical point detector selected for use in SPIDAR was the lightweight chemical detector (LCD-3™) available from Smiths Detection, shown in Figure 1. The LCD detector is a pulse inlet ion mobility spectrometer (IMS) that samples the air for chemical agents, toxic industrial chemicals, and simulants. Ion mobility spectra in positive and negative modes are provided every five seconds. An intensive analysis of individual LCD responses to simulants, independently confirmed through simultaneous quantification with gas chromatography, led to the development of compound-specific regression equations for use in an effective calibration scheme. In addition, the calibration scheme employs reduced mobility to correct IMS drift time responses for environmental factors such as temperature and pressure.

Figure 1. Lightweight Chemical Detector (LCD) from Smiths Detection.

The weather station selected for use in SPIDAR was the Airmar Weather Station LB100 / PB100 (Airmar), shown in Figure 2. The weather station provided meteorological data and an integrated global positioning system (GPS) receiver. Ethernet connectivity for SPIDAR components was provided by the Digi Port Server TS-2 H MEI serial port server and connected the sensors to the SPIDAR Base Station for data retrieval and command and control. In the first tests series each of the 25 stations communicated through the center station back to the SPIDAR Base Station, whereas in the second test series each station communicated directly to the SPIDAR Base Station.

Figure 2. The Airmar Weather Station PB100.

The other sensing component developed for the RTVS test grid was an array of irregularly spaced, standoff IR sensors developed by ECBC and Physical Sciences, Inc. Looking in towards the test grid, the IR sensors were able to observe the space above the grid to a height over 100 meters. The 5-member IR sensor grid consisted of a passive multispectral imaging system referred to as "AIRIS," for Adaptive Infrared Imaging Spectroradiometer. An AIRIS sensor is shown in Figure 3.

Figure 3. Two views of an AIRIS sensor.

An AIRIS sensor is based on a long-wavelength IR (LWIR) focal plane array-based camera that enables radiance measurements of sufficient accuracy for species-specific

6

column densities of chemical clouds to be determined. A low-order, tunable Fabry-Perot etalon provides the spectral resolution necessary to resolve structured absorption and emission from molecular vapors. Optically, the AIRIS sensors generated images of 256 × 256 pixels with a field-of-view of 30 degrees by 30 degrees. The spectral coverage available was from 7.9 μm to 11.2 μm at roughly 0.1 μm resolution. The outputted data consisted of 20 wavelengths acquired and processed every 2 seconds (0.5 Hz).

In addition to the RTVS sensor systems, several sensor systems from Dugway's referee system were active during testing [2, 3]. Three infrared Orion 890VL Radiometer-Tracker Interface systems (i.e., infrared cameras) were placed around the grid. Radiometer data were recorded and processed to generate three-dimensional positional data and contour models for detected simulant clouds. MESH, Inc. provided six scanning Fourier-transform infrared (FTIR) chemical cloud tracking systems (CCTS) placed around the grid similar to the AIRIS systems. After processing, the MESH FTIR system provided two-dimensional composite views of simulant clouds scaled to concentration intensity. The grid size employed by the FTIR system was significantly larger and of a coarser resolution than that of AIRIS.

The referee point chemical detection system consisted of multiple ppbRAE detectors from RAE Systems collocated with the LCD point sensors. In contrast to the IMS technology used in the LCD detectors, the ppbRAE systems were based on photoionization sensing technology and were designed for the detection of volatile organic compounds.

Dugway also supplied meteorological systems for the test grid. These included a 32 m tower instrumented with temperature sensors, a Sonic Detection and Ranging (SODAR) system, and several Portable Weather Information Display Systems (PWIDS) dispersed across the test grid that supplied general meteorological information.

3. METHOD

3.1. Data Fusion

Intelligent data fusion offers the possibility of viable multisensory solutions built with commercial-off-the-shelf or custom sensing components for both real-time and retrospective applications. Successful data fusion depends on more than just increasing the number of sensors, which often increases false positives in lockstep with detections [4]. Rather, the design of an effective multisensor detection system hinges on careful choice of sensing hardware, its respective sensor response characteristics, as well as the relationship between the sensors and the events to be detected. Additional key challenges include establishing an appropriate frame of discernment for the sensing problem, leveraging decision-level data from available sensor algorithms, and properly addressing data disparity in fused systems.

First, for the purposes of this discussion, a multisensor detection system is one that is comprised of several component sensing elements, the outputs of which are combined together with signal processing, feature extraction, and data fusion algorithms to produce a quantitative (or qualitative) assessment of the current sensing task. Potential applications of multisensor systems include chemical sensing, explosives detection, fire detection, situational awareness, and many other sensing tasks [5]. There are several potential benefits to a multisensor approach: by combining data from multiple, orthogonal sources of information, multisensor systems can demonstrate improved selectivity, accuracy, and reliability when compared to single sensor systems in terms of enhanced detection capabilities, reduced false positives, and decreased missed detections. The utilization of multiple sensing elements can also lead to enhanced system robustness and fault tolerance.

Multisensor systems come with their own set of unique challenges, however. The first of these is addressing data disparity in a multimodal sensing system. In a typical multisensor system, such disparity may be as simple as varied spatial positioning among sensor elements, or as complex as gross differences in both the format of the sensor output and in the fundamental type of information the sensor supplies. Selecting optimal types, locations, or numbers of sensors is highly dependent on the sensing task and may be mitigated by external factors such as deployment restrictions, computational complexity, or available resources. A further challenge is that merely adding sensors will not necessarily result in improved system performance. For example, a simulation of ten identical binary sensors, shown in Figure 4, demonstrates that a simple Boolean "AND" combination of the sensor outputs resulted in lower detection rates than those obtained using a single sensor, while a Boolean "OR" resulted in higher false positive rates. Thus, an increase in the detection rate will likely be accompanied by an unacceptable increase in false positives unless sensor data are combined using intelligent data fusion algorithms that optimize sensor performance in a fused system. Effective, reliable sensors are commercially available for a multitude of sensing tasks, but these sensors are often designed for single sensor environments and binary "threat" or "no-threat" output.

8

Therefore a further challenge unique to multisensor systems is leveraging decision-level data from available sensor algorithms.
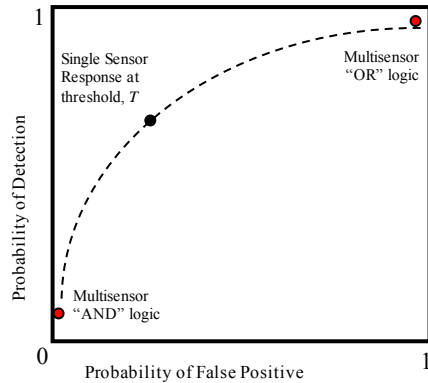
Figure 4. ROC curve for a single binary sensor overlaid with response characteristics for a simulated network of ten identical sensors combined with Boolean logic.

The development of a multisensor system is an iterative process and includes a number of key ingredients, each of which are partially dependent on the others. The first of these is defining a frame of discernment, which makes explicit the sensing tasks to be accomplished. Next is the selection of sensors suitable for the chosen frame of discernment. Different sensing modalities should be included to provide complementary information that addresses challenges posed by the frame of discernment or limitations posed by sensors of a single modality. Issues with available sensors may force a refinement in the frame of discernment. Next is the development of relevant feature sets from sensor data. Commercial sensors with smart algorithms should be properly leveraged for optimal benefit. Finally, features and data should be integrated with data fusion algorithms. NRL has found that a modular design to system architecture, together with a tiered approach to algorithmic analysis, to be most useful for developing effective multisensor systems.

In a multisensory system, data disparity can manifest in several ways. Individual sensing units may be spatially separated from one another within a monitored space, or may display temporal disparity, acquiring readings at different times or with different frequencies. In these cases, data registration techniques must be employed. More severe are situations involving different sensing modalities, in which there is disparity between the form of the sensor output (for example, the combination of binary and continuous output sensors), or in the type of information that is being presented (for example, the combination of light sensors and microphone outputs). In these cases, data processing and feature extraction techniques must be used to extract relevant information from the sensor outputs to which the data fusion algorithms can be tailored.

Approaches to data fusion generally fall into one of the following categories: 1) heuristic/ rule based algorithms that involve construction of a logical decision tree that encodes known relationships between sensors and detectable events, 2) pattern recognition algorithms that operate on data vectors consisting of aggregate sensor and algorithm output, 3) Bayesian theoretic algorithms that take advantage of knowledge regarding the

statistical relationship between collected sensor outputs and detectable events, 4) Dempster-Shafer theoretic algorithms that are based on subjective assessments of belief that specific sensor outputs convey, and 5) hybrid algorithms consisting of some combination of these approaches.

For instance, specific heuristic rules can come from theoretical or empirically derived expert knowledge regarding sensor response characteristics and sensor-to-sensor relationships. While a heuristic approach is simple computationally and allows for detailed input of known relationships between sensor responses and detectable events, it also leads to complexity in the design process, inability to capture hidden relationships, and to a lack of flexibility that makes heuristic rules difficult to implement with data sets that vary in format and composition over time.

Pattern recognition techniques include classification algorithms such as linear discriminant analysis (LDA) and probabilistic neural networks (PNN), as well as numerous others [6]. These techniques can act as data fusion algorithms when they are applied to a vector of aggregated sensor responses. In and of themselves, they have limited capabilities to address data disparity, but can represent a potent means of discovering hidden relationships between sensor data and detectable events given appropriate data preprocessing and proper training with experimental data.

Bayesian reasoning and Bayesian belief network architectures are powerful tools for inductive reasoning within a probabilistic framework [7, 8]. The core of the Bayesian approach was formulated from Bayes" rule, shown in eq. (1), which states that for a hypothesis, H, and evidence, E, the probability of the H, conditioned on E is given by

$$p(H|E) = p(H) \times \frac{p(E|H)}{p(E)} \tag{1}$$

The first term, p(H), is the prior probability of H and represents knowledge of H before observing evidence E. The second term is the normalized likelihood and represents knowledge of how likely it is to observe E, given H. Multiplication of these two terms provides the posterior probability of H, given observed evidence E. If multiple lines of evidence, $E = \{e_1, e_2, e_3, \dots e_n\}$, are available, the joint distributions must be considered, $p(\{e_1, e_2, e_3, \dots e_n\}|H)$ and $p(\{e_1, e_2, e_3, \dots e_n\})$.

Fortunately, in many cases calculating the joint distribution of several variables is made simpler by examining the causal relationships among the variables and identifying those that are independent. A specification of these relationships and the conditional probability values associated with them forms what is known as a Bayesian belief network. A further simplified "naïve" Bayesian approach is to assume independence amongst each line of evidence, as in eq. (2).

10

$$p(\{e_1, e_2, e_3, . . e_n\}|H) = \prod_{i=1}^{n} p(e_i|H) \qquad (2)$$

The initial prior probability for H can be updated to a posterior probability of H by consecutively multiplying it by the normalized likelihood of each available line of evidence, $p(e_i|H) / p(e_i)$, for $i \in \{1 \ldots n\}$.

Briefly, Dempster-Shafer theory can be described as a generalization of Bayes theory in which observed evidence can support not only specific hypotheses, but also sets of hypotheses [5, 9]. Dempster-Shafer data fusion has been utilized in applications such as land cover classification, machine vision, and medical diagnoses [10, 11, 12]. The approach is attractive for problems involving evidence pooling from multiple sources because it does not require complete specification of the underlying conditional probabilities and it allows for assignment of a degree of belief to a specific hypothesis without necessarily assigning any belief to the negation of that hypothesis. These properties enable Dempster-Shafer frameworks to address evidence associated with subjective uncertainty in a more satisfying manner than a Bayesian approach while simultaneously retaining the ability to incorporate evidence associated with objective uncertainty [13].

In Dempster-Shafer theory, the evidence observed from a given sensor response provides support for one or more of the elements of the frame of discernment including, potentially, supersets combining two or more elements. A unit probability mass is apportioned across the elements (and sets of elements) for which the sensor's response provides support. The amount of mass assigned to any given focal element is representative of the relative amount of certainty with which the sensor response can make that declaration. Mass assigned to a superset of all unique elements in the frame of discernment represents the degree to which the data are uncertain in providing support for any particular element.

Probability mass assignments from multiple information sources are pooled according to Dempster's rule of combination, which amounts to a calculation of the cross products of the probability mass assignments for each data source. Each cross product is assigned to a hypothesis that represents the intersection of the two component probability masses used to generate it. Cross products assigned to the same hypothesis are summed, resulting in a series of unique output hypotheses with corresponding probability mass assignments. If any cross products result from conflicting hypotheses, they are removed from the set and the remaining masses are normalized to sum to unit mass. Such renormalization has the effect of redistributing the mass assigned to conflict proportionally across the remaining hypotheses.

In the example shown in Figure 5, evidence from two sensors providing support for varying elements in the frame of discernment (labeled A, B, C, and D) is pooled according to Dempster's rule. The net effect is the assignment of most of the probability mass to element A (=0.56), a reduction of those assigned to the set of elements A and B (=0.24) and A and C (=0.14), as well as a reduction of the mass assigned to uncertainty (=0.06).

11

$m_1(A,B)=0.8$

Sensor 1

$m_1(A,B,C,D)=0.2$

$m_{1,2}(A)=0.56$ $m_{1,2}(A,B)=0.24$

$m_{1,2}(A,C)=0.14$ $m_{1,2}(A,B,C,D)=0.06$

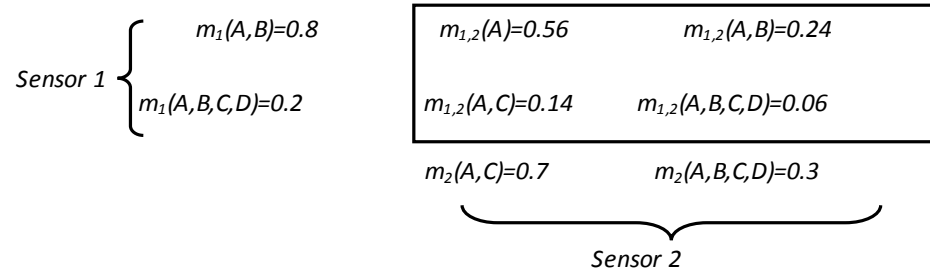$m_2(A,C)=0.7$ $m_2(A,B,C,D)=0.3$

Sensor 2

Figure 5. Hypothetical example of Dempster-Shafer fusion of evidence provided by two disparate sensors.

4. EXPERIMENTAL

As part of the program, two field tests were conducted to evaluate the RTVS detection systems (LCD and AIRIS) and contrast their performance against the legacy Dugway systems (ppbRAE and MESH). Both test series were conducted at the US Army"s Dugway Proving Ground in Utah and consisted of successive releases of various chemical agent simulants under several dissemination scenarios. Two different test grids were used for the field tests. The first test series (RTVS "07) was performed at Dugway"s V-Grid, during the nights of 17 – 21 September 2007 [2]. The second test series (RTVS "08) was at Dugway"s S-Grid, during the nights of 09 – 19 June 2008 [3]. The layout for the detection systems was similar for both test series. Point sensors with collocated weather stations were distributed near ground level at locations across a square grid. The standoff sensors were distributed roughly symmetrically around the square grid of point sensors, but at distance of 1 – 3 km from grid center. Data acquired by the sensors were relayed wirelessly to an on-site command post for processing and logging. Dissemination locations for the simulants were also located more than 1 km distant from grid center, but were clustered near the central axis of the test grid. Test scenarios were conducted by Dugway personnel. A typical testing procedure consisted of 10 – 20 minutes of background data collection followed by the release of one (or more) simulants and continued data acquisition. The cessation of data acquisition, after anywhere from 15 – 60 minutes, constituted the end of an individual test scenario. Set up for the next test scenario was conducted after determination of a safe all-clear environment by Dugway testing personnel.

4.1. RTVS '07 Test Series

The first RTVS test series was conducted 17 – 21 September 2007 on Dugway"s V-Grid. The layout of the grid, RTVS and Dugway detection systems, weather stations, and simulant dissemination locations are shown in Figure 6. The core of V-Grid was a square of 1 km per side rotated approximately 15 degrees clockwise from true north. The 25 RTVS point sensors (SPIDAR LCD"s) were distributed at a height of 1 meter equitably in nine rows across this core grid (see Figure 7 for positions and labels of the LCD sensors). SPIDAR Airmar weather stations were also located coincident with all LCD detectors at a height of about 1.5 meters. The five RTVS standoff sensors (AIRIS) were positioned 2.7 km from grid center. Wide area AIRIS detectors were placed (see Figure 6) at the Northwest, East, and South positions while tomographic AIRIS detectors were placed at the Northeast and Southeast positions.
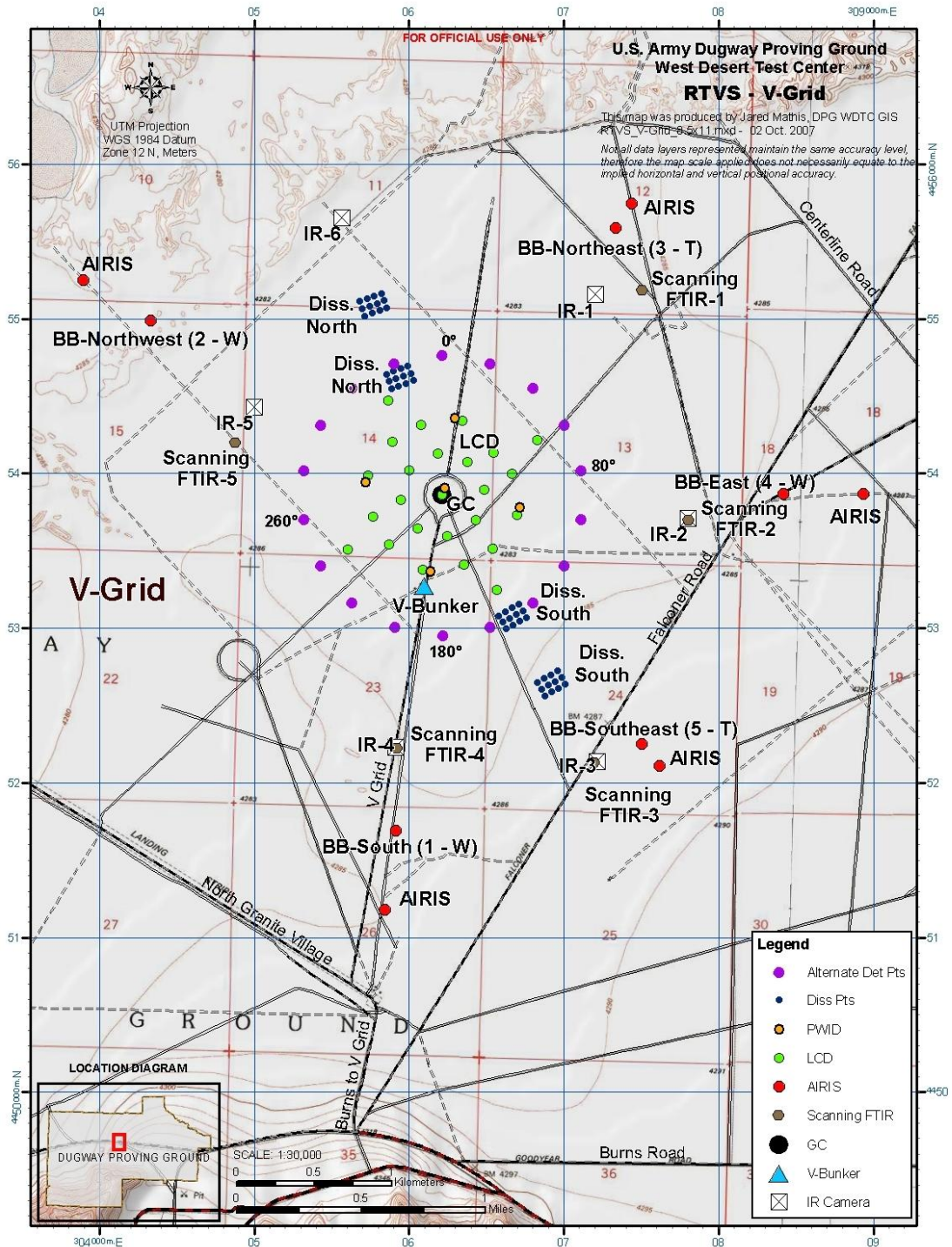
Figure 6. Target V-Grid, Dugway Proving Ground, UT. AIRIS – Adaptive Infrared Imaging Spectroradiometer sensors; IR – Orion infrared cameras; Diss. Pts – dissemination points for chemical simulants; FTIR – MESH scanning Fourier-transform infrared (FTIR) sensors; LCD – SPIDAR Lightweight Chemical Detectors; GC – grid center; Det Pts – detonation points; PWID – Portable Weather Information Display System; BB – reference blackbody reflector for AIRIS; T – tomographic AIRIS; WAD – wide area detector AIRIS; (not shown) – ppbRAE point sensors at various LCD locations

14
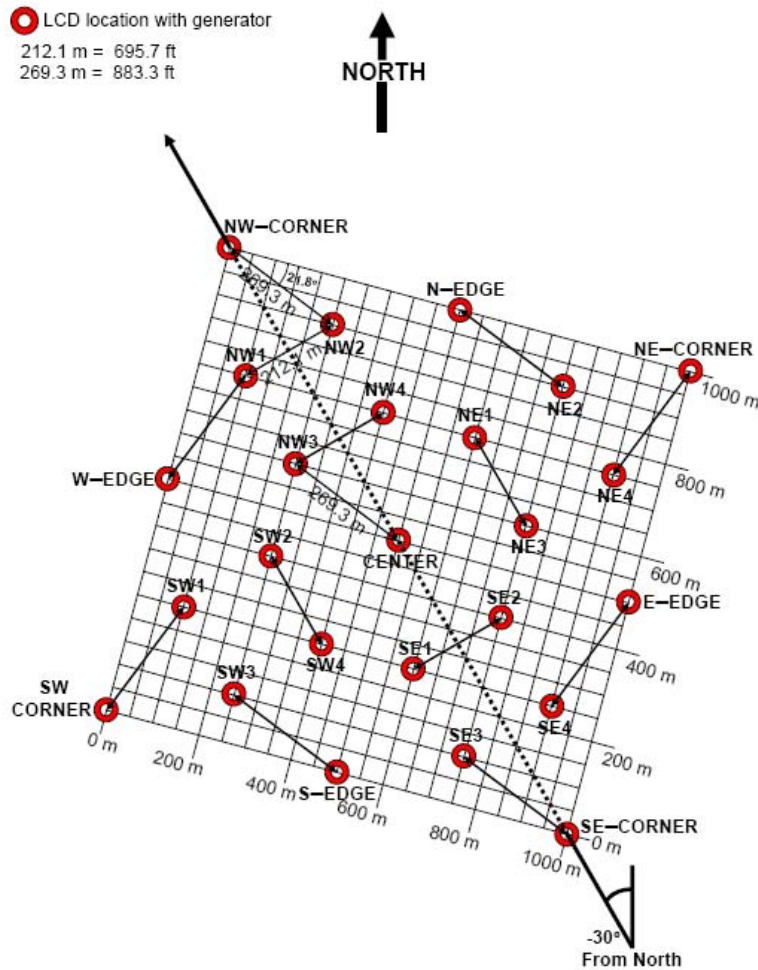
Figure 7. Positions and labels of LCD detectors and Airmar weather stations on V-Grid for the RTVS '07 test series.

For the Dugway standoff detection systems, five scanning FTIR systems (MESH) were placed (see Figure 6) roughly coincident with the AIRIS systems, but located generally nearer to grid center. A total of three Orion IR cameras, at six locations, were used. Five of the locations were with the scanning FTIR systems, and the sixth was located northwest of the core grid roughly halfway between IR-1 and IR-5. Thirteen Dugway point sensing systems (ppbRAE) were placed coincident with the RTVS point sensors, of these only seven were calibrated and used during any given test. The selection of RTVS point sensor locations at which to place coincident ppbRAE sensors was varied for each testing day (see [2]). Five PWIDS weather stations were placed in the core grid. One PWIDS was located at grid center and the other four were located at the midpoints of the 1 km sides of the core grid square.

Only one chemical simulant, triethyl phosphate or TEP, was released during the RTVS "07 test series. A total of twelve release scenarios were conducted with the amount of

TEP released varying from 10 to 160 kg. Dissemination was performed using explosive detonation at three locations: northwest of the test grid 2 – 2.5 km from grid center (two tests), southeast of the test grid 2 – 2.5 km from grid center (seven tests), and at a third location southwest of the grid (five tests). Liquid TEP in plastic jugs was placed on C4 explosive and a blasting cap was used to achieve detonation, which both vaporized the simulant and pushed it high into the air. Table A1 in the Appendix gives a summary of the tests run during RTVS07.

Data acquired by the sensing systems was transmitted wirelessly from the location of acquisition to a command post located about 1 km south of the core grid. The hardware was specified by Dugway for secure wireless transmissions. For the LCD point sensors, acquired data were minimally processed by the sensors themselves before secure transmission in real-time to the command post. There, software developed by the SPIDAR team running on a PC-grade workstation processed the data for heads-up display and logged it for later analysis. For the AIRIS sensors, the volume of acquired data was far in excess of the capacity of the wireless system. Thus, AIRIS data were processed and stored by a PC-grade notebook located at each acquisition site. An abbreviated version of the data was transmitted in real-time to the command post where software developed for AIRIS running on PC-grade workstations processed the data for heads-up display. The heads-up display provided 2-D horizon views from each reporting AIRIS sensor and also estimates of the three dimensional spatial extent of the simulant cloud and its concentration profile.

Data from the LCD sensors and Airmar weather stations were made available in one large ASCII (text) file. Individual sensors were identified by location (northing, easting) and time stamp. Post-processing was employed with the AIRIS data to perform three-dimensional tomographic reconstruction of the simulant clouds. Data were reconstructed into a cube comprised of $256 \times 256 \times 256$ voxels (i.e., a 3-D volume element analogous to 2-D pixels.) Ground level in the reconstructed data cube corresponded to all voxels in z-bin 128 (i.e., $x \times y \times 128$ for $(x, y) \in 1:256$). Post-processed data were made available as: (1) JPEG images of the 2-D views from each of the five AIRIS sensors, (2) a series of JPEG images showing the 3-D simulant cloud against easting, northing, and vertical z coordinate axes at various time stamps, and (3) as a binary file containing the detected concentrations in each voxel of the data cube at all reconstructed times.

4.2. RTVS '08 Test Series

The second RTVS test series was conducted 09 – 19 June 2008 on Dugway"s S-Grid. The layout of the grid, RTVS and Dugway detection systems, weather stations, and simulant dissemination locations are shown in Figure 8. The core of S-Grid was a square of 1 km per side rotated approximately 5 degrees clockwise from true north. The 25 RTVS point sensors (SPIDAR LCD"s) were distributed at a height of 1 meter across this core grid (see Figure 8) as in the earlier test series (see Figure 7). SPIDAR Airmar weather stations were also located coincident with all LCD detectors at a height of approximately 1.5 meters. The five RTVS standoff sensors (AIRIS) were positioned 2.7

km from grid center. The distribution of the AIRIS systems around grid center was not entirely symmetric. A gap in coverage occurred northeast of the grid, opposite AIRIS-3.

For the Dugway standoff detection systems, five scanning FTIR systems were placed (see Figure 8) around the core grid, however only one (FTIR-2) was roughly coincident in field of view with an AIRIS system (AIRIS-3). A total of six Orion IR cameras were used, five of which were located coincident with the scanning FTIR systems, and the sixth was located northwest of the core grid on the grid diagonal. Fifty Dugway point sensing systems (ppbRAE) were placed coincident with the RTVS point sensors, two per LCD location. The paired ppbRAE systems were placed on a single mast at heights of 1 and 6 meters. Five PWIDS weather stations were placed in the core grid. One PWIDS was located at grid center and the other four were located at the midpoints of the 1 km sides of the core grid square.

Three chemical simulants were released during the RTVS '08 test series: triethyl phosphate (TEP), methyl salicylate (MeS), and acetic acid (AA). A total of 29 release scenarios were conducted: fifteen TEP releases of 30 – 150 kg, seven MeS releases of 30 – 150 kg, two MeS/TEP joint releases of 30 and 75 kg each, four AA releases of 30 – 150 kg, and one "blank" scenario consisting of a dust cloud without any simulant. Dissemination was performed using explosive detonation (as in RTVS '07) at two of three northern dissemination sites (eight tests total at N2 and N3), all of the southern grids (17 tests total at S1, S2, and S3), and at an additional west center location used for stack releases (four tests). During a stack release, liquid simulant was continuously pumped through a shaft attached to a crane and then vaporized about 20 meters above ground. A stack release typically lasted fifteen minutes. Table A2 in the Appendix gives a summary of the tests run during RTVS08.

Data acquired by the sensing systems was transmitted wirelessly from the location of acquisition to a command post located about 1 km south of the core grid. For RTVS '08 however, Dugway provided a different hardware system, Cisco 1300 series radios, for secure wireless transmissions. The data assimilation, display, and logging systems employed for the SPIDAR LCD point sensors, Airmar weather stations, and AIRIS standoff sensors were essentially identical to RTVS '07. For RTVS '08, the LCD data were post-processed to remove transient duplicate points. Data were made available in the same text-based format. AIRIS data were post-processed as for RTVS '07, but the reconstructed 3-D data cubes was made available in a sparse matrix format, which greatly reduced the file sizes.
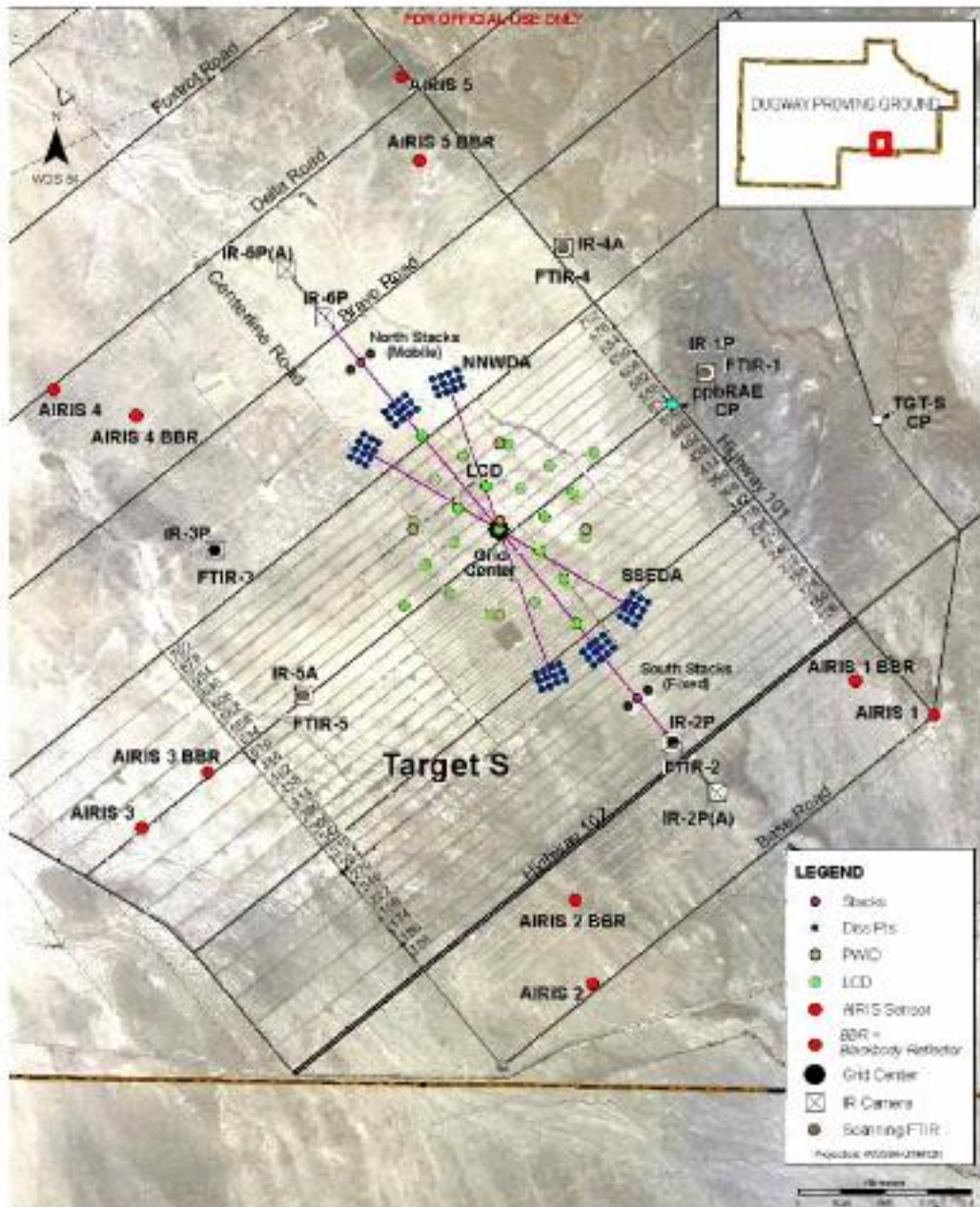
Figure 8. Target S, Dugway Proving Ground, UT. AIRIS – Adaptive Infrared Imaging Spectroradiometer sensors; IR – Orion infrared cameras; Diss. Pts – dissemination points for chemical simulants; NNWDA – north northwest dissemination area; SSEDA – south southeast dissemination area; FTIR – MESH scanning Fourier-transform infrared (FTIR) sensors; LCD – SPIDAR Lightweight Chemical Detectors; PWID – Portable Weather Information Display System; BBR – reference blackbody reflector for AIRIS; (not shown) – two ppbRAE point sensors at each LCD locations; numbers 126 through 702 are road numbers.

5. RESULTS AND DISCUSSION

5.1. RTVS '07 Test Series

The September 2007 RTVS test series was the first time the RTVS sensor systems had been assimilated and field tested as a group. During testing at Dugway, winds were light and variable, which made simulant releases difficult. Acquired data were also limited due to issues with the communications network. As a whole, the test series served primarily as a necessary shakeout for the newly developed data acquisition, communications systems, and testing methods. Areas for improvement were identified and test data were made available for preliminary data fusion studies exploring data registration and feature selection strategies for the RTVS data.

During testing the SPIDAR LCD detectors had difficulties communicating in real-time with the command post over the wireless network. The source of the problem was suspected to be a strong radar source that knocked out the system during setup and caused it to run at a reduced capacity for the remainder of the test series. Table 1 indicates from which LCD detectors data were received for each of the twelve tests. A total of six to seven LCD detectors reported data consistently for every test, while one to two additional detectors reported partial data for some tests. Therefore, data were obtained from only about a third of the LCD detectors. LCD data were supplied in text format as chemical type and detected concentration as a function of time. Figure 9 shows the detected concentrations as a function of time of four LCD detectors, those at SW Corner, Center, NE 1, and NE 3, to two similar 30 kg TEP simulant releases from the southwest. These were the only LCD detectors to respond during these tests and transmit data. The initial strong and persistent simulant signals observed at the SW Corner closest to the release point have been dispersed or have not reached far across the grid, most likely due to weak winds. The final test of the series, test #13T160, a release of 160 kg TEP from the southeast, better demonstrates the potential for a grid of point sensors such as the LCD detectors. The responses, shown in Figure 10, follow the simulant cloud from the southeast as it moves across the grid and dissipates.
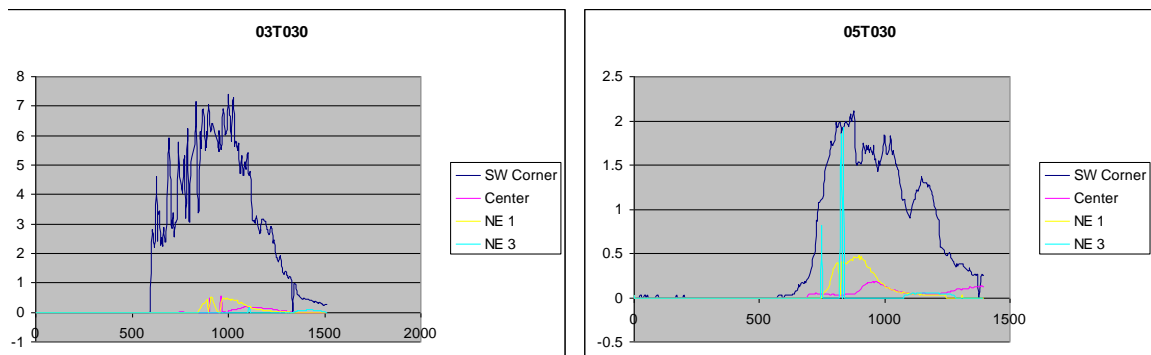

Figure 9. Examples of LCD readings versus time for two similar 30 kg TEP releases from southwest of the grid.

Table 1. Limits of data obtained for LCD detectors on V-Grid for the RTVS '07 test series

Location\Test #	1	3	4	5	6	7	8	9	10	11	12	13
NW Corner	✓	?	✗	✓	✓	✓	✓	✓	✓	✓	✓	✓
N Edge	✗	✗	✗	✗	✗	✗	✗	✗	✗	✗	✗	✗
NE Corner	✗	✗	✗	✗	✗	✗	✗	✗	✗	✗	✗	✗
W Edge	✗	✗	✗	✗	✗	✗	✗	✗	✗	✗	✗	✗
Center	✓	✓	✓	✓	✓	✓	✓	✓	✓	✓	✓	✓
E Edge	✗	✗	✗	✗	✗	✗	✗	✗	✗	✗	✗	✗
SW Corner	✓	✓	✓	✓	✓	✓	✓	✓	✓	✓	✓	✓
S Edge	✗	✗	✗	✗	✗	✗	✗	✗	✗	✗	✗	✗
SE Corner	✗	✓	✓	✓	✓	✓	✗	✓	✓	✗	✗	?
NW1	✗	✗	✗	✗	✗	?	✗	✗	✗	✗	✗	✗
NW2	✗	✗	✗	✗	✗	✗	✗	✗	✗	✗	✗	✗
NW3	✗	✗	✗	✗	?	✗	✗	✗	✗	✗	✗	?
NW4	✗	✗	✗	✗	✗	✗	✗	✗	✗	✗	✗	
NE1	✓	✓	✓	✓	✓	✓	✓	✓	✓	✓	✓	✓
NE2	✗	✗	✗	✗	✗	✗	✗	✗	✗	✗	✗	✗
NE3	✓	✗	✓	✓	✗	✓	✓	✓	✓	✓	✓	✓
NE4	✗	✗	✗	✗	✗	✗	✗	✗	✗	✗	✗	✗
SW1	✗	✗	✗	✗	✗	✗	✗	✗	✗	✗	✗	✗
SW2	?	✗	✗	✗	✗	✗	✗	✗	✗	?	✗	✗
SW3	✗	✗	✗	✗	✗	?	✗	✗	✗	✗	✗	✗
SW4	✗	✓	✗	✗	✗	✗	✗	✗	✗	?	✗	✗
SE1	✗	✗	✗	✗	✗	✗	✗	✗	✗	✗	✗	✗
SE2	✗	?	✗	✗	✗	✗	✗	✗	✗	✗	✗	?
SE3	✗	✗	✗	✗	✗	✗	✗	✗	✗	✗	✗	✗
SE4	✓	✓	✓	✗	✓	✓	✓	✓	✓	✓	✓	✓
✓	6	6	6	6	6	7	6	7	7	6	6	6
?	1	2	0	0	1	2	0	0	0	2	0	3

✓	Data for entire test
?	Data for only part of test
✗	No Data

13T160
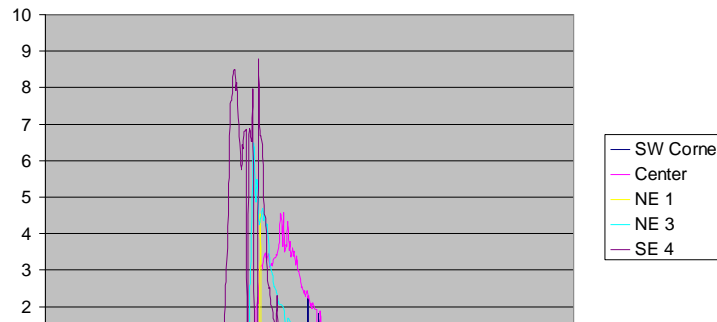
Figure 10. Example of LCD readings versus time for a 160 kg TEP release from southeast of the grid.

In general, the AIRIS standoff detectors responded well to the TEP releases. The response of the AIRIS detectors approximately 10 minutes after the release of 100 kg of TEP simulant is shown in Figure 11 and Figure 12. AIRIS data were supplied in binary and image formats. Figure 11 is an example of image data displaying five real time 2D views from the AIRIS detectors. The 2D view displays the cross sectional area perpendicular to that AIRIS instrument"s field of view with the horizon line roughly bisecting the middle of the image. In the 2D view, detected simulants were shown as colored pixels while an estimate of the concentration detected was supplied in the lower left of the image. Figure 12 shows an example of 3D image data constructed retrospectively from the individual 2D views using computational tomography [14]. The figure displays the reconstructed simulant cloud together with its projections in the northing (x), easting (y), and horizontal (z) planes. These projections also show the concentration of the column density. The entire reconstructed data cube consisting of $256 \times 256 \times 256$ voxels as a function of time was supplied in a binary file. Each voxel contained the concentration for that location in space and step in time. These data were used for data fusion development.

Figure 11. Two-dimensional sensor views of the AIRIS detectors' responses approximately 10 minutes after the release of 100 kg TEP. The red pixels indicate the extent of the detected simulant cloud. Sensors 1, 2, and 4 were the newer wide-area type. Sensors 3 and 5 were the older tomographic type.
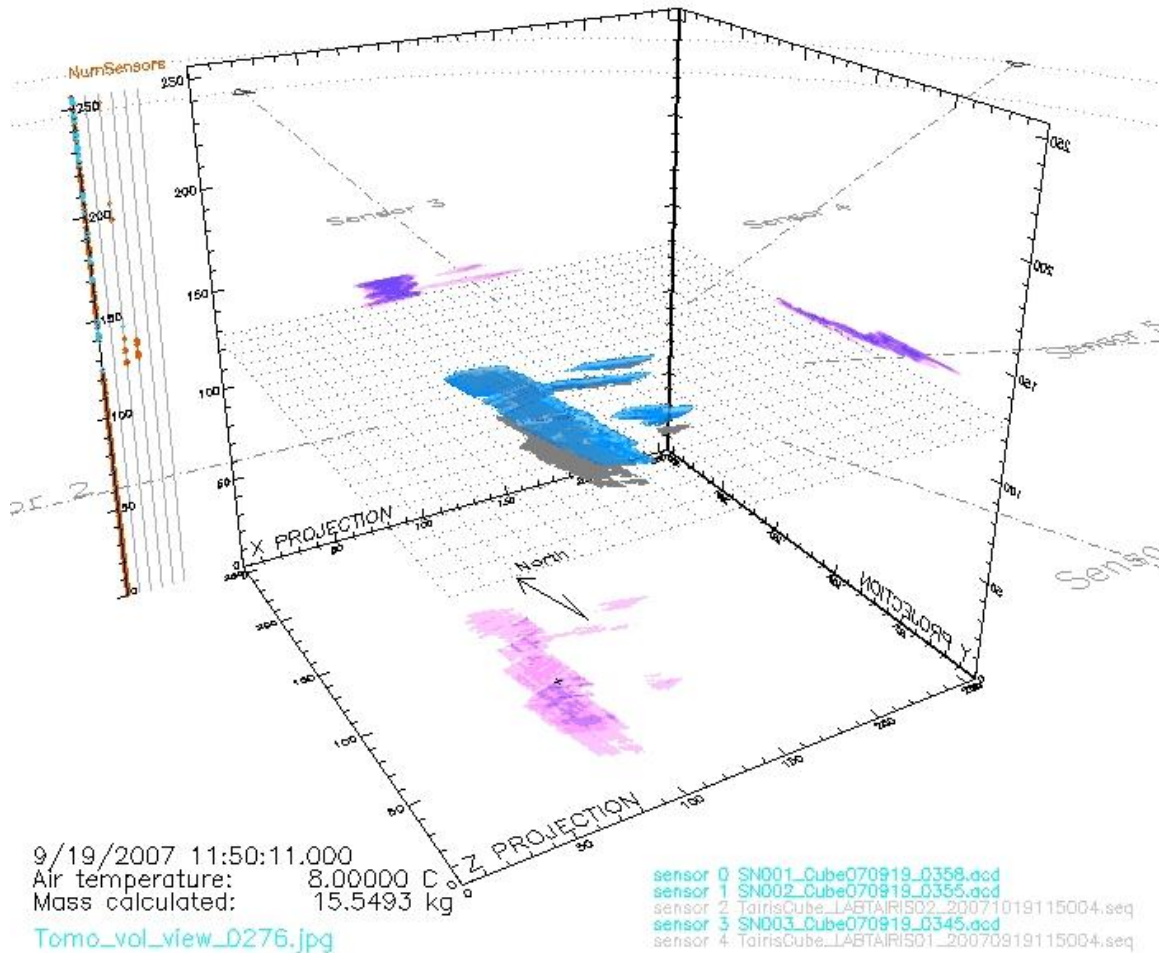
Figure 12. Tomographically constructed three-dimensional view of the AIRIS detectors' responses approximately 10 minutes after the release of 100 kg TEP. Ground level is shown in blue shading with projections in lavender shading.

As for weather data during RTVS ′′07 testing, the communications issues meant that even fewer SPIDAR Airmar weather stations than LCD detectors were able to report to the command post. The Airmar weather stations were administered by the SPIDAR team and transmitted data simultaneously with the LCD systems. Only the weather station located at the Center location reported data consistently for the test series. Partial data was received from a few other Airmar weather stations (one to four) for portions of some of the tests. Measured weather data were temperature, pressure, relative humidity, wind speed, and wind direction, but were only compiled during active data acquisition (i.e.,

during testing). The recorded pressures were not calibrated correctly for the height above sea level at V-Grid and required correction using the formula given in eq. (3),

$$P_{alt}(h) = P_{station} \bigg/ \left(\frac{288 - 0.0065h}{288}\right)^{5.2561} \qquad (3)$$

Here h is the height above sea-level (i.e., altitude) in meters and $P_{station}$ is the barometric pressure measured at the weather station. The altitude of the center station was 1305.97 meters. P_{alt} is the resulting altitude-corrected, barometric pressure.

A much better weather dataset was provided by the five Dugway PWIDS weather stations. Measured weather data were of the same type: temperature, pressure, relative humidity, wind speed, and wind direction, as the Airmar weather stations, but data were supplied at intervals of 10 seconds for the entire two-week testing period. Figure 13 displays the temperature, pressure, and relative humidity data obtained from the five PWIDS weather stations overlaid together with its maximum variance as a function of time for the week of data taking, 09/16/2007 – 09/21/2007. The data vary significantly as a function of time over the day / night cycle and given weather patterns. However for a given time selection, these data are remarkably consistent between PWIDS stations, indicating that there was little variation in temperature, pressure, or relative humidity with respect to grid location, at least at ground level.

Because the Airmar stations were less sophisticated instruments and had not been used before, there was some question as to the efficacy of their data. To test this, weather data acquired from the Airmar stations, where available, were compared to those obtained from PWIDS. Figure 14 shows a comparison of the temperature, pressure, and relative humidity data from the PWIDS and Airmar weather stations collocated at grid center during the week of testing. The data are sufficiently consistent with each other, given the difference in cost between the two types of weather stations.
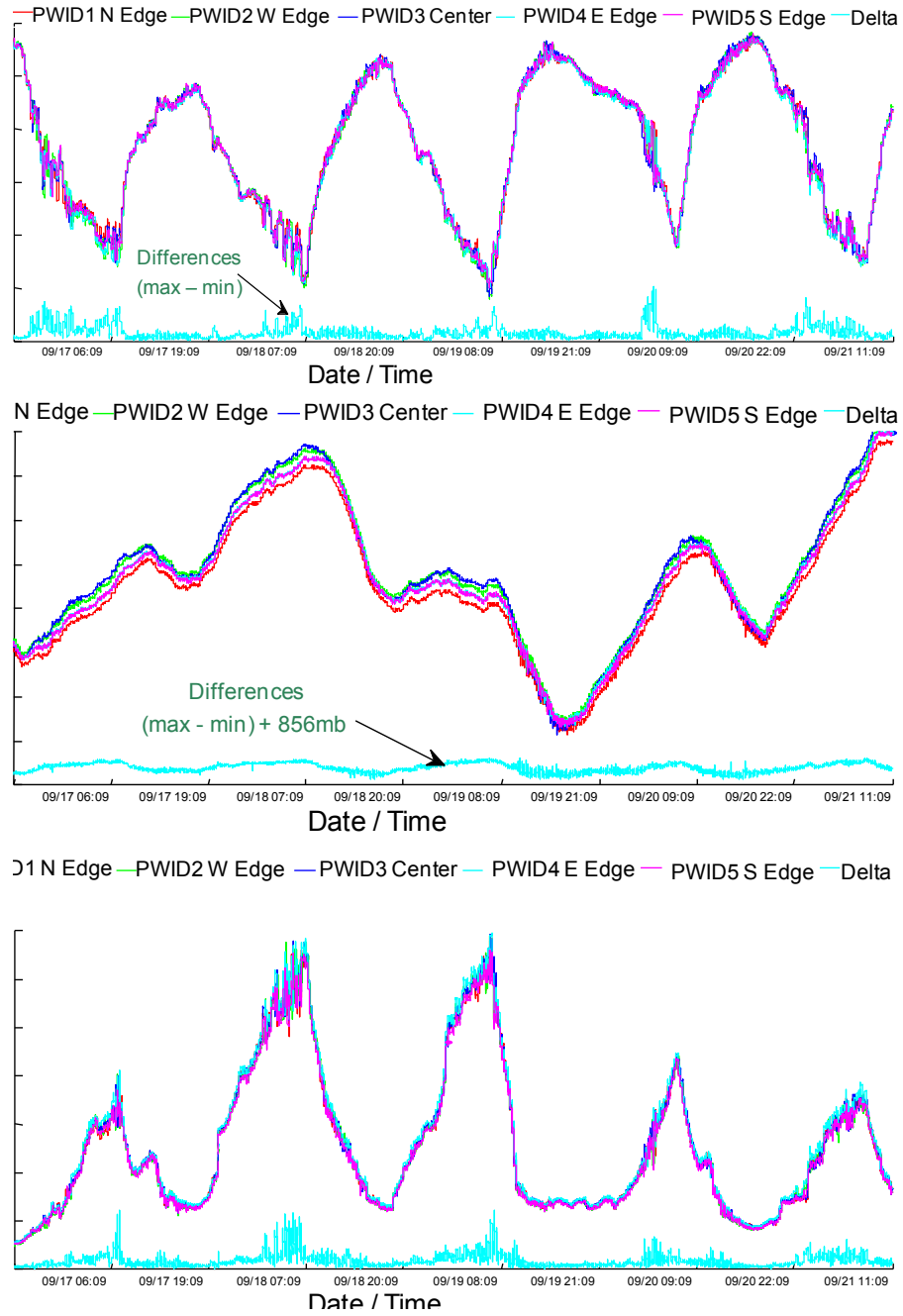
Figure 13. Overlays of temperature, pressure, and relative humidity weather data from the five PWIDS weather stations for the dates 09/16/2007 – 09/21/2007.
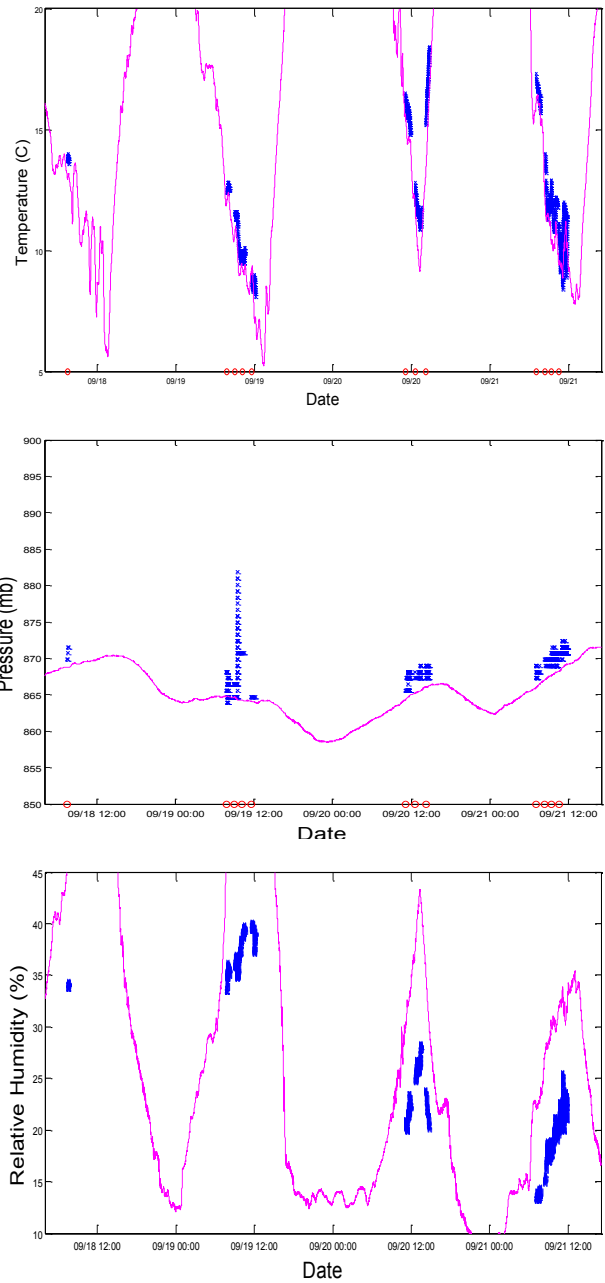
**Figure 14. Comparison of temperature, pressure, and relative humidity weather data
from the PWIDS (magenta line) and Airmar (blue crosses) weather stations
collocated at grid center. The red circles mark the start times for the 13 tests.**

5.2. RTVS '08 Test Series

The June 2008 RTVS test series was much more successful than the 2007 test series in
terms of the quantity and quality of data collected by the RTVS sensor systems and the

number and variety of tests performed. Environmental conditions on Target S were more stable, which made possible more simulant releases. Issues with a new wireless communications network supplied by Dugway were quickly resolved. A larger data set of higher quality was acquired and made available for data fusion algorithm development.

Between the 2007 and 2008 test series, the SPIDAR team had tested a new access point wireless communications system in the field at Dugway in order to resolve the issues that had compromised data acquisition for the LCD detectors and Airmar weather stations. However, the communications hardware selected and tested by SPIDAR did not meet evolving security requirements for wireless systems at Dugway in time for the 2008 test series. Therefore, Dugway provided an alternative, but slower, point to multi-point wireless system for sensor communications. During test set up and shakedown, several communications issues developed with the SPIDAR systems due to the interaction of low-level driver software supplied by Smiths Detection with the less capable Dugway wireless system. The SPIDAR resolved the issues by modifying their software to more closely supervise wireless transmissions, ensuring that all data from all detectors was transmitted sequentially to the base station. By the end of the first week, more than 20 LCD detectors were reporting completely, although this was achieved by sacrificing the data from the weather stations to minimize the data traffic on the network. An additional issue was that the LCD data were observed to have occasional dropouts, that is, gaps in the time series data, which were due to a software problem that was found and corrected.

Once the communications issues were resolved, nearly all the LCD detectors were reporting valid streams of data during testing. The same single file, text-based data format was used for data logging, though without the file locking issues observed in 2007. Figure 15 shows the responses of the LCD detectors (blue) to an explosive release of 150 kg of TEP. The responses are shown as concentrations (mg/m^3) versus time after release (minutes). The placement of the graphs in the figure corresponds to the locations of the LCD detectors on the test grid. As a group, the response of the LCD detectors is consistent with that of a simulant cloud drifting across the grid from the northwest (upper left) to the southeast (lower right). In Figure 15, the numbers in the upper left of the graphs indicate the onset of detection in minutes for the LCD at that location. Times for the leftmost graphs were 1.2 min, 6.9 min, and 3.5 min for locations NW-Corner, NW-1, and NW-3, respectively. (See Figure 7 for LCD location identifiers.) Times for the rightmost graphs were 7.0 min (N-Edge), 2.6 min (NE-2), 4.1 min (NE-4), and 6.7 min (E-Edge). Finally, the LCD at SE-Corner, located furthest from the simulant source, detected the release after 22.8 min. While the general results were consistent with a simulant cloud drifting across the grid from the northwest to the southeast, the variations in incipient LCD detection times and missing detections indicated that the cloud dispersal was not linear across the grid at ground level despite relatively uniform wind speeds and directions.
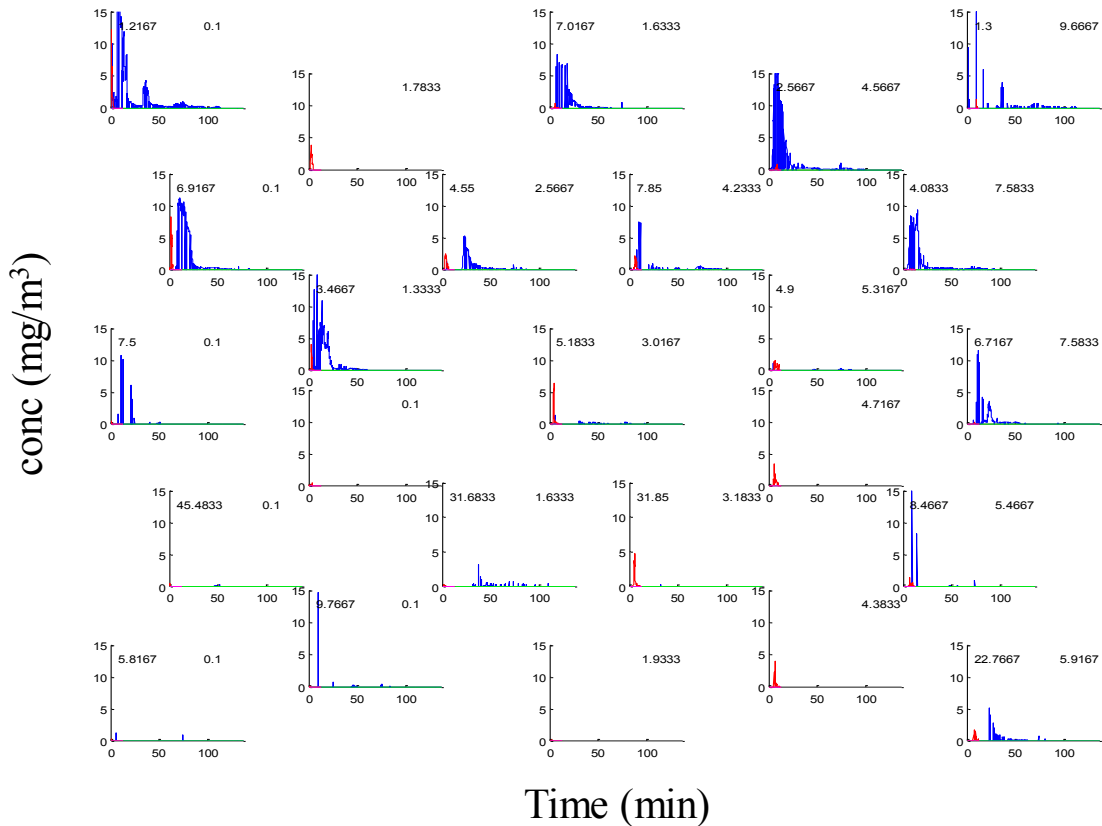
Figure 15. Comparison of LCD (blue) and AIRIS (red) responses versus time after release for a 150 kg explosive release of TEP (test #05T150). The placement of the graphs corresponds to the LCD grid locations. The numbers indicate the start times for TEP detection for LCD (left) and AIRIS (right).

The performance of the AIRIS systems during the 2008 test series was similar to that of 2007. However, during the first week of testing, one of the AIRIS sensors failed, followed by another unit during the second week. The format of the image data was identical to that of 2007. The binary data format was improved by using a compression algorithm to remove redundancies and significantly decrease the file size required to store the voxel data cubes. (Most AIRIS voxels had values of zero.) As in 2007, only 2D data were available in real-time. The 3D voxel data cubes were retrospectively reconstructed from the 2D data.

One of the new developments for the 2008 test series was a „stack release" where liquid simulant was piped to a point high above ground and then vaporized. A stack release efficiently supplied a constant stream of simulant for cloud formation at an altitude much easier to detect with standoff sensors than had been observed with ground-based explosive releases. Figure 16 shows the response of the AIRIS detectors (red) to a 30 kg stack release of TEP (test #10T030). The format is identical to that of Figure 15, and the incipient detection times for AIRIS are provided in minutes in the upper right of the graphs. In addition, the AIRIS responses shown correspond to the altitude layer at that LCD location for which the detected concentration was largest (i.e., the largest detected coincident AIRIS response). As in the earlier test, the results were consistent with a simulant cloud dispersing across the test grid in a non-linear manner both spatially and

27
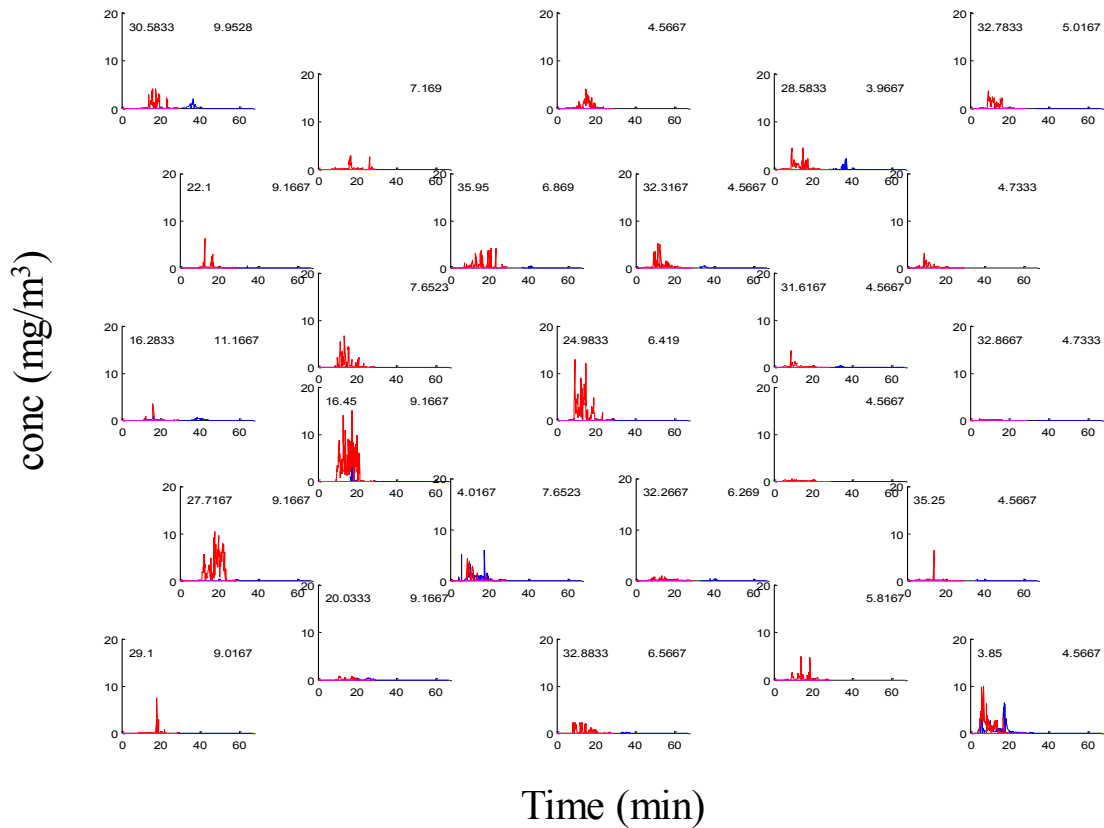
Figure 16. Comparison of LCD (blue) and AIRIS (red) responses versus time after release for a 30 kg stack release of TEP (test #10T030). AIRIS data are the maximum concentration over all levels at that LCD grid location. The numbers indicate the start times for TEP detection for LCD (left) and AIRIS (right).

temporally. Further, the much weaker LCD responses (blue) and much later incipient times (10 to 20 minutes) were consistent with non-linear cloud dispersion all the way down to ground level.

As in the 2007 test series, weather data in the 2008 test series were acquired via the 25 SPIDAR Airmar and the five Dugway PWIDS weather stations. Weather data reporting was more successful for SPIDAR in 2008 than in 2007, with little variation from the PWIDS. Similar agreement as with 2007 data was observed in the temperature, pressure, and relative humidity data, and similar variance was observed in wind speeds and directions, which certainly contributed to the non-linear dispersion of the simulant cloud.
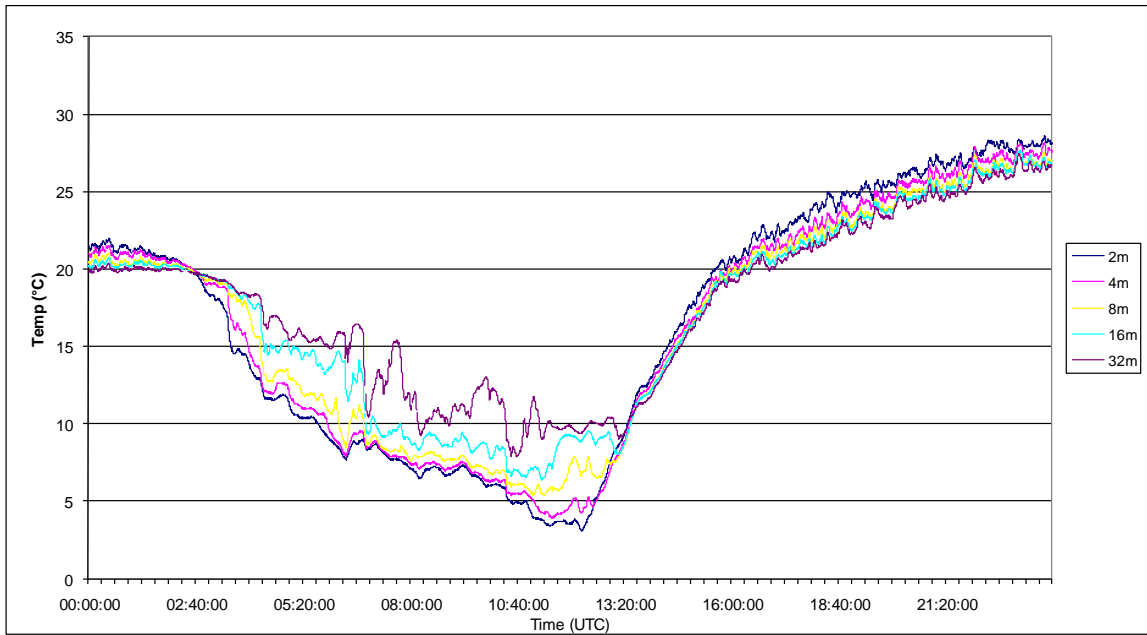
Figure 17. Temperature data in degrees Celsius versus time at heights of 2 m, 4 m, 8 m, 16 m, and 32 m recorded at center grid location on 06/13/2008.
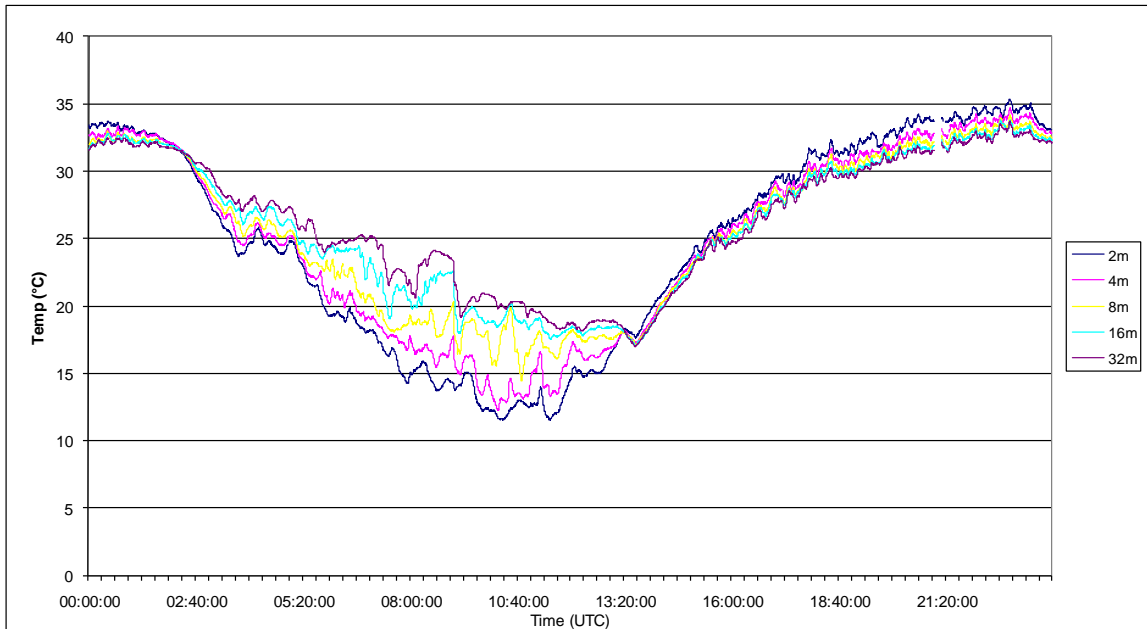
Figure 18. Temperature data in degrees Celsius versus time at heights of 2 m, 4 m, 8 m, 16 m, and 32 m recorded at center grid location on 06/16/2008.

New for the 2008 test series was the 32 m tall mast at the center grid location. The mast was instrumented with temperature sensors at heights of 2 m, 4 m, 8 m, 16 m, and 32 m above ground level and provided data at ten second intervals for all test days. Figure 17 and 18 display temperature data collected on the center mast for the days of 06/13/2008 and 06/16/2008 in UTC time, respectively. Local time is UTC time minus six hours. That is, midnight in the figure is 6 pm local time. The wide band on the left

side of the figures corresponds to night; the narrower band on the right side with day. During the day the temperature variance with respect to height had a maximum of about 3 °C from ground level to the top of the mast. However, at night, when most RTVS testing occurred, the temperature variance was much larger (up to 10 °C) and inverted (coolest at ground level). The standoff IR sensors, such as AIRIS and MESH FTIR, depend on an accurate measurement of the ambient air temperature in order to detect interesting foreground deviations (i.e., potential chemical clouds) from ambient background. During the RTVS test series, the standoff IR systems relied on temperature measurements made at ground level, which have shown little variance with location (see Figure 13). The demonstrated variance with height may have adversely impacted the measurements made by the IR systems for regions of the sky several meters above ground level. For instance, Figure 19 displays the temperature dependence of the blackbody radiation curve at temperatures of 11 °C and 15 °C for infrared wavelengths. The maximum variation of intensity with respect to wavelength occurs in the infrared.
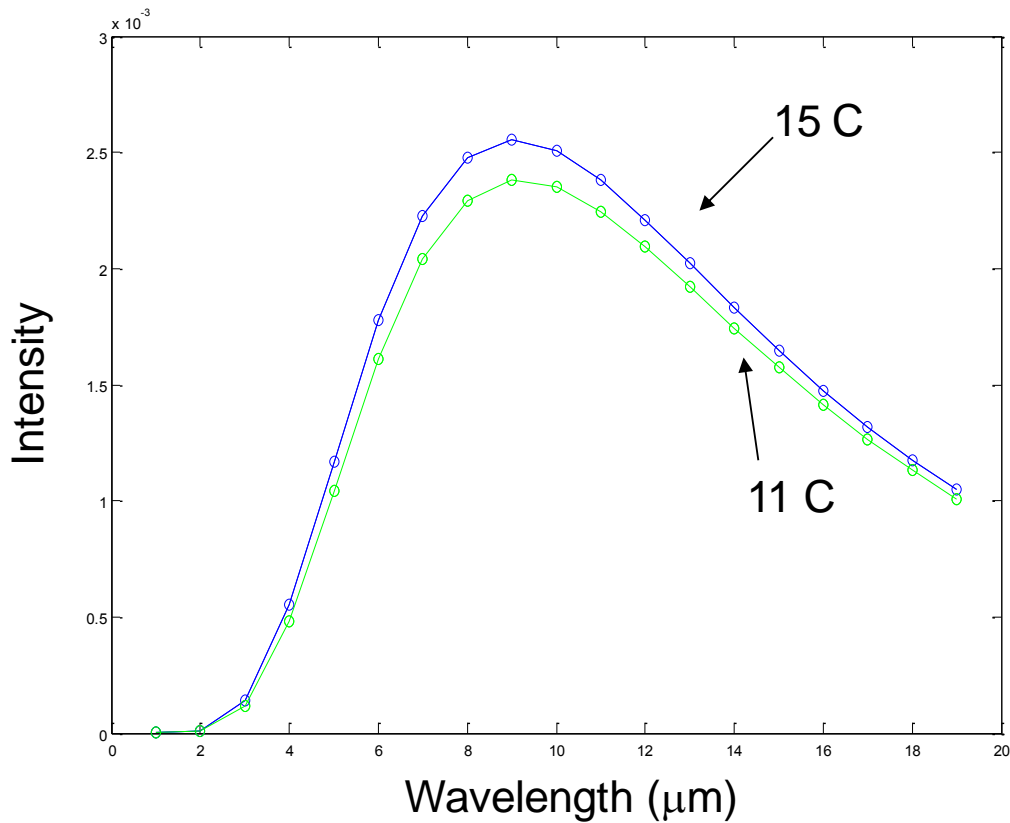
Figure 19. Blackbody radiation curves for temperatures of 11 °C and 15 °C.

5.3. Data Fusion

5.3.1 Data Assimilation

From the perspective of data fusion, the RTVS analysis presented several challenges. The first of these was that the RTVS sensors were disparate in modality, location, and number. Standoff and point-type sensors acquired concentration and class data at different rates from a number of spatial locations. A strategy was developed for a common spatial and temporal approach to the sensor data from which a higher-level analysis on the combined dataset could be performed.

The spatial resolution of the data at ground level is shown in Figure 20 in northing and easting coordinates for the V-Grid from the 2007 RTVS testing. Here, the black circles indicate the locations of the LCD and ppbRAE detectors on the test grid. The densely hatched blue lines indicate the pixels (4 m × 4 m) of the AIRIS standoff sensors. As part of the tomographic reconstruction, the extent of AIRIS coverage was intentionally restricted to the test grid. The larger green lines indicate the pixels (50 m × 50 m) of the MESH FTIR standoff sensors. (Processed FTIR data actually consisted of 15 m × 15 m pixels, a finer resolution than shown.) Increased coverage area is a tradeoff with pixel resolution, as shown in Figure 21, a zoomed version of Figure 20 that displays a detailed view of the respective standoff sensor pixel areas surrounding a single point sensor location. The spatial description of the RTVS sensor data for V-Grid is functionally identical to Target-S from 2008.
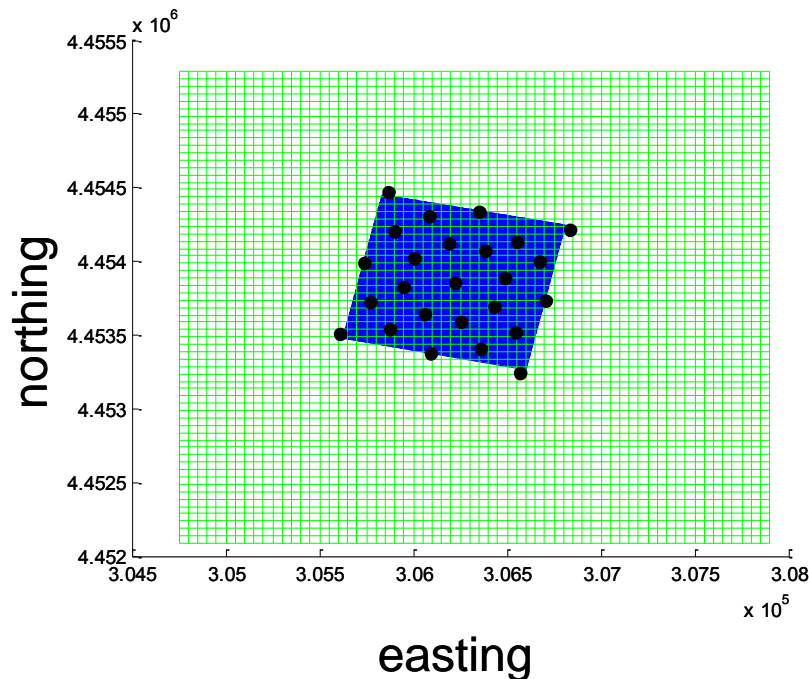
Figure 20. Locations of LCD point sensors (black circles), AIRIS (blue lines) and FTIR (green lines) grids – wide-area view.
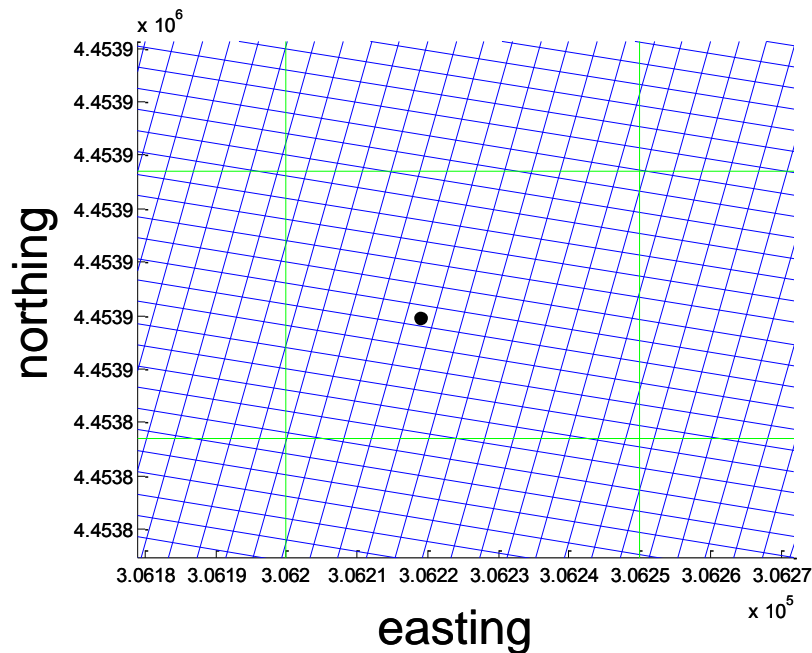
Figure 21. Locations of LCD point sensors (black circles), AIRIS (blue lines) and FTIR (green lines) grids – zoom view.

The AIRIS sensors provided a third spatial dimension of concentration data indexed by height above the test grid. Tomographic reconstruction generated 3D voxels of dimension 6 m in height, (i.e., the *z*-direction). Although the data cube contained 256 voxels in *z*, referred to as *z*-bins, the layout of the source images restricted their output to bins 128 to 255, equivalent to ground level to a maximum height of over half a kilometer. A 3D diagram of the AIRIS voxels is shown in Figure 22. The test grid and LCD locations are shown at ground level and the grid lines correspond to the vertical layers of AIRIS voxels. Together, ground level sensors and the reconstructed AIRIS data provided a three-dimensional view of the test grid that tracked the extent and movement of the simulant cloud across the grid. Note also that three-dimensional data were not available for the MESH FTIR sensors. Rather, FTIR data were compressed to a 2D layer for single, representative time slices and supplied as images not suitable for computer-based
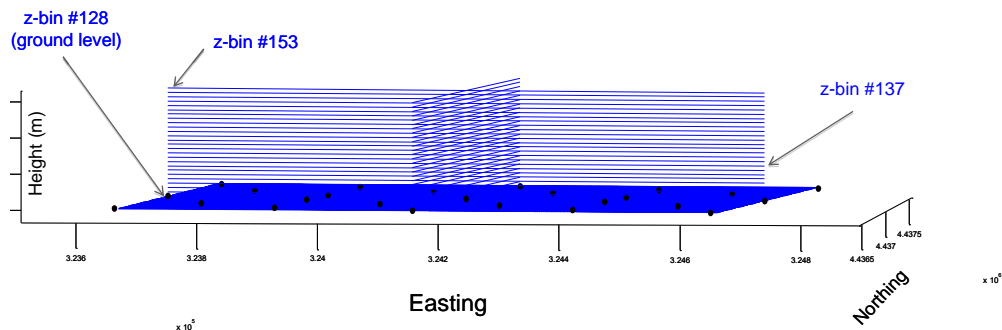
Figure 22. AIRIS *z*-bins.

analysis.

A temporal description of the RTVS data is supplied in Table 2. The time resolution of the data is listed in hertz and seconds for the various sensors. The LCD provided data points at 5-second intervals. The AIRIS system processed data at 2-second intervals in real time (listed as „raw"), but the resolution of the supplied data cube was reduced to 10-second intervals after tomographic reconstruction (listed as „processed"). For comparison, the time resolution of the Dugway legacy ppbRAE point sensors was 10-second intervals, and for the FTIR standoff sensors, 30-second intervals. Note that the time-resolved data from the FTIR sensors were not available. Only 2D images at selected time-slices were published. The time resolution of the weather data was 5 seconds for the LCD stations and 10 seconds for the Dugway PWIDS stations.

Table 2. Data acquisition rates.

System	Frequency (Hz)	Time (s)
LCD	0.2	5
AIRIS (raw)	0.5	2
AIRIS (processed)	0.1	10
ppbRAE	0.1	10
FTIR (processed)	0.03	30
LCD Weather Stations	0.2	5
PWIDS Weather Stations	0.1	10

Temporally, the RTVS datasets were registered to a common time grid with a 10-second resolution, matching that of the AIRIS and ppbRAE data. The LCD data were interpolated to a 10-second resolution using an industry standard, spline-based interpolation technique provided by Matlab"s „interp" family of functions [15]. Spline-based interpolation is well suited for relatively well-behaved data (e.g., continuously differentiable), such as the RTVS data.

Spatially, the RTVS datasets were analyzed in two different modes: columnar and layered. In the columnar approach, the AIRIS standoff data were compared to the point sensor data at each of the 25 locations (see Figure 7). For this analysis, the set of AIRIS data voxels that formed the entire column of data above each location was compared to the LCD and ppbRAE data at ground level for that location. In the layered approach, the LCD data were compared to the ground level layer of the AIRIS data and nearby layers above ground level. For this analysis, a layer of point sensor data with the same spatial resolution as the AIRIS data were constructed from the LCD data by interpolating spatially across the locations separately for every point in time. Spline-based interpolation techniques, as in the temporal interpolation described above, were employed. Results from these analyses were presented as movies constructed from images of the combined data at various time steps. These results are discussed further below.

5.3.2 Data Quality

The second challenge for the RTVS data fusion analysis was to capture and leverage as much information as possible from the sensor algorithms themselves. Fundamental to this effort was the evaluation of the quality of the datasets, their consistency and their reproducibility in response to varying levels of simulants. The development of the RTVS sensors incorporated sophisticated methods for calibration, data acquisition, and data processing that ideally, were the best available for their respective instruments. Successful fusion with data obtained from multiple sensing modalities (e.g., RTVS standoff and point sensors) requires a solid understanding of the resulting data quality in order to limit uncertainties that may be magnified into erroneous information by data fusion algorithms further up the processing stream.

Overall, the LCD detectors and AIRIS sensors were consistently responsive to the TEP and MeS simulants. The sensor responses were not in general smooth, but were observed to be somewhat choppy and intermittent, which can be seen in a close examination of the concentration profiles of Figure 9, Figure 10, Figure 12, Figure 15, and Figure 16, for example. There was some question as to whether or not the AIRIS sensors were detecting much of the simulant clouds from explosive releases, but as the AIRIS response was quite similar to that of the MESH FTIR standoff sensors, and both responded much stronger to simulant from stack releases, it appears safe to conclude that the lack of data points was mostly an artifact of the dissemination method and not due to an ineffective calibration of the standoff sensors.

The effort put forth to develop a rigorous and sensible method for calibrating the LCD detectors appears to have paid off in reproducible data with a consistent baseline and predictable response across the test grid and simulant classes. A consistent baseline was observed to be quite a problem with the ppbRAE detectors whose response was frequently shifted by amounts on the order of the concentrations measured. The effect was particularly prominent in the 2007 V-Grid tests. For the 2008 Target-S tests, the response of the ppbRAE detectors was less than desired to the TEP and MeS classes and baseline problems continued. Note that the ppbRAE detectors responded well to acetic acid, as shown in Figure 23, though baseline problems are apparent. The LCD sensors were not configured to detect acetic acid.

34
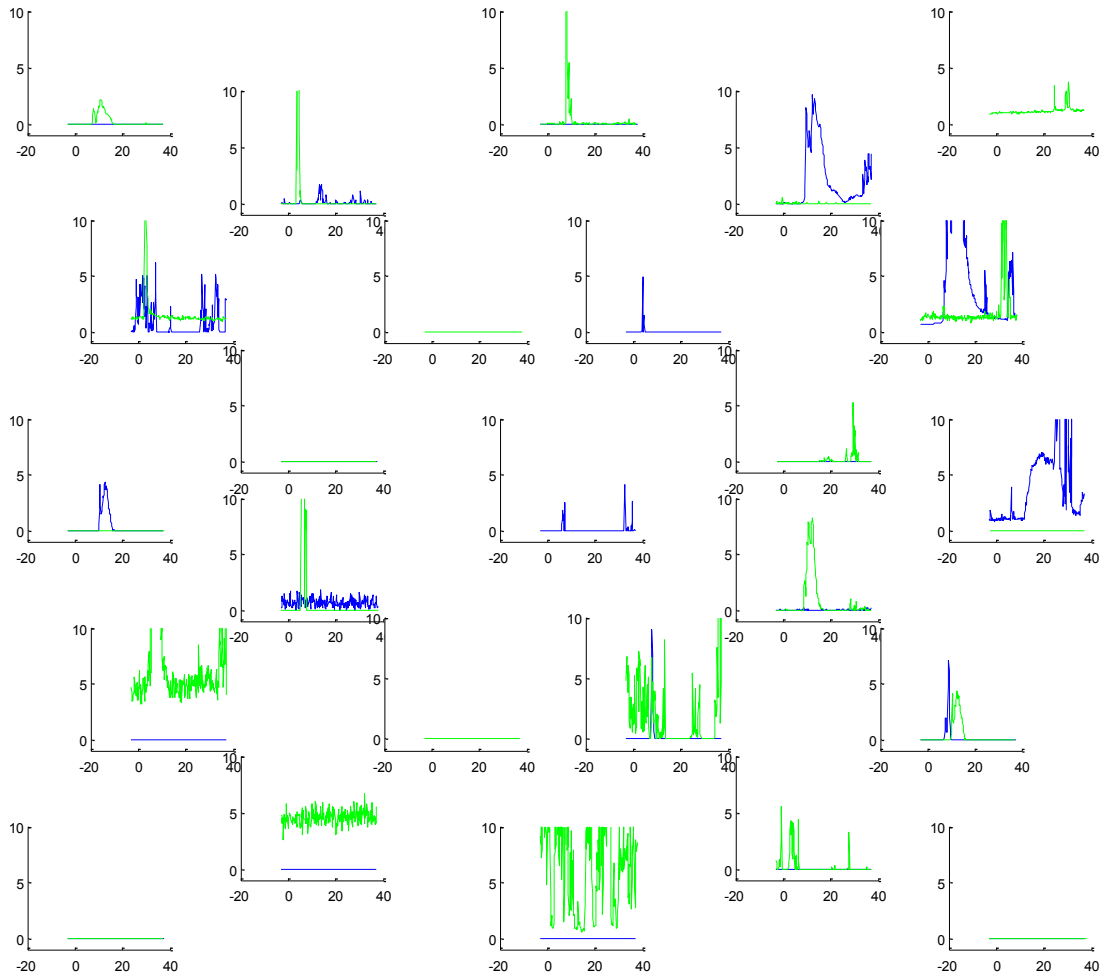
Figure 23. Response of ppbRAE detectors to acetic acid in test #36AA075. The upper ppbRAE detector is in blue, the lower in green.

The temperature gradient with respect to height above ground, shown in Figure 17 and Figure 18, may have affected the calibration and responses of the AIRIS and MESH IR sensors, which rely on an accurate measurement of the background ambient air temperature in order to detect and measure foreground features. Ambient temperature values also appear in a number of the equations used in tomographic reconstruction. However, a direct estimate of the effect of an erroneous ambient temperature is difficult to determine without modeling the entire reconstruction procedure using pure input and output signals of varying intensities.

Some issues were observed with the consistency of the data obtained from all sensor systems. For example, the response of an LCD detector occasionally appeared to erroneously drop to zero. These phenomena appeared to be a general characteristic of the LCD sensor responses rather than a problem with an individual malfunctioning detector. Data dropouts caused discontinuities in the concentration profiles and were problematic for the temporal and spatial interpolation, which was how they were uncovered.

A further aspect to be considered with the consistency of the data was its variability, and the implications of those variances for false positives and false negatives. Here, false positives are defined as incorrect indications of a threat (incorrect detections), and false negatives as incorrect indications of the absence of a threat (incorrect all-clear signals). As mentioned earlier, sensor responses were generally not smooth, but often choppy with a significant variance. Figure 15 shows the concentration profiles (blue) from several LCD detectors, nearly all of which exhibit a large variance. (Note for comparison, the LCD concentration profile shown in Figure 24 is considered to be smoothly varying, particularly after dropout correction (bottom)). Figure 16 shows concentration profiles (red) from several individual AIRIS voxels coincident with LCD detectors. These profiles also exhibit a significant variance.
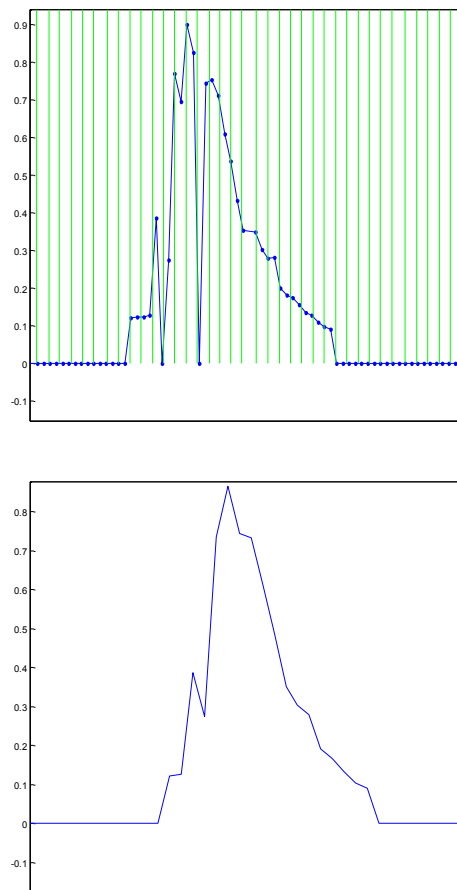
Figure 24. (Top) Example of LCD data (blue dots) with dropouts, timescale grid (green lines) of 10-second resolution. (Bottom) LCD data after correction and interpolation.

36

The tomographic reconstruction methods employed by the AIRIS and MESH FTIR sensor systems also introduced a large number of artifacts into the standoff data. Figure 25 shows the reconstructed AIRIS voxels, color-coded by z-bin level. The regions of detection show hard boundary edges in line formations that are coincident with the locations of the AIRIS sensors. The coincidence is evidence that the line features are artifacts due to the reconstruction, rather than detected features of the simulant cloud. Gaps and additions along these line features may also be artifacts of the reconstruction algorithms. Figure 26 shows four different time slices of FTIR data from test #10TE030. The green dots represent the locations of the FTIR sensors and the white lines radiating from these locations provide an indication of each sensor"s field of view relative to the reconstruction. Evidence for linear features, gaps, and other areas of potential added material, is easier to discern in these images. A likely explanation is that one of the sensors detected some level of simulant in a particular pixel in its 2D view, but the reconstruction algorithms were not able to determine accurately where that simulant measurement was located with respect to the other sensors. Therefore, uncertainty remained as to how far away from the sensor the simulant was detected. Compounding these uncertainties across all of the 2D data leads to observed artifacts in the reconstructed 3D data. Note that similar artifacts were observed with both the AIRIS and MESH FTIR data even though different reconstruction algorithms were employed. Tomographic reconstruction in three dimensions is by nature an ill-posed inversion problem that is only made more difficult when variances are present in the 2D source data.

Data variance and artifacts need be understood and quantified for effective data fusion. In standard signal processing analysis, the variance of a signal is considered a good indication of the inherent uncertainty of that signal. That is, a large variance implies a large uncertainty in any sample data point. With respect to the RTVS sensors, however, the impact of several factors on data variance must also be evaluated. These factors include environmental conditions at the test site, the dissemination methods used to generate the simulant clouds, and the interactions of these with characteristics of the sensors themselves. Columnar and planar analyses were used to investigate these factors.

As mentioned earlier, a columnar analysis was performed by examining the sensor data at the locations of the 25 LCD detectors. At the bottom of the data column (ground level), there were data from the LCD detector and the lowest AIRIS voxel in the column. The remainder of the data column consisted of the other 127 AIRIS voxels coincident with the LCD detector but increasing in height z to the top of the AIRIS data cube. It was expected that a simulant cloud passing through such a data column would exhibit connectivity between voxels adjacent in height, and if coincident with ground level, the LCD detector as well. Little evidence for connectivity or coincidence was observed in the RTVS data.
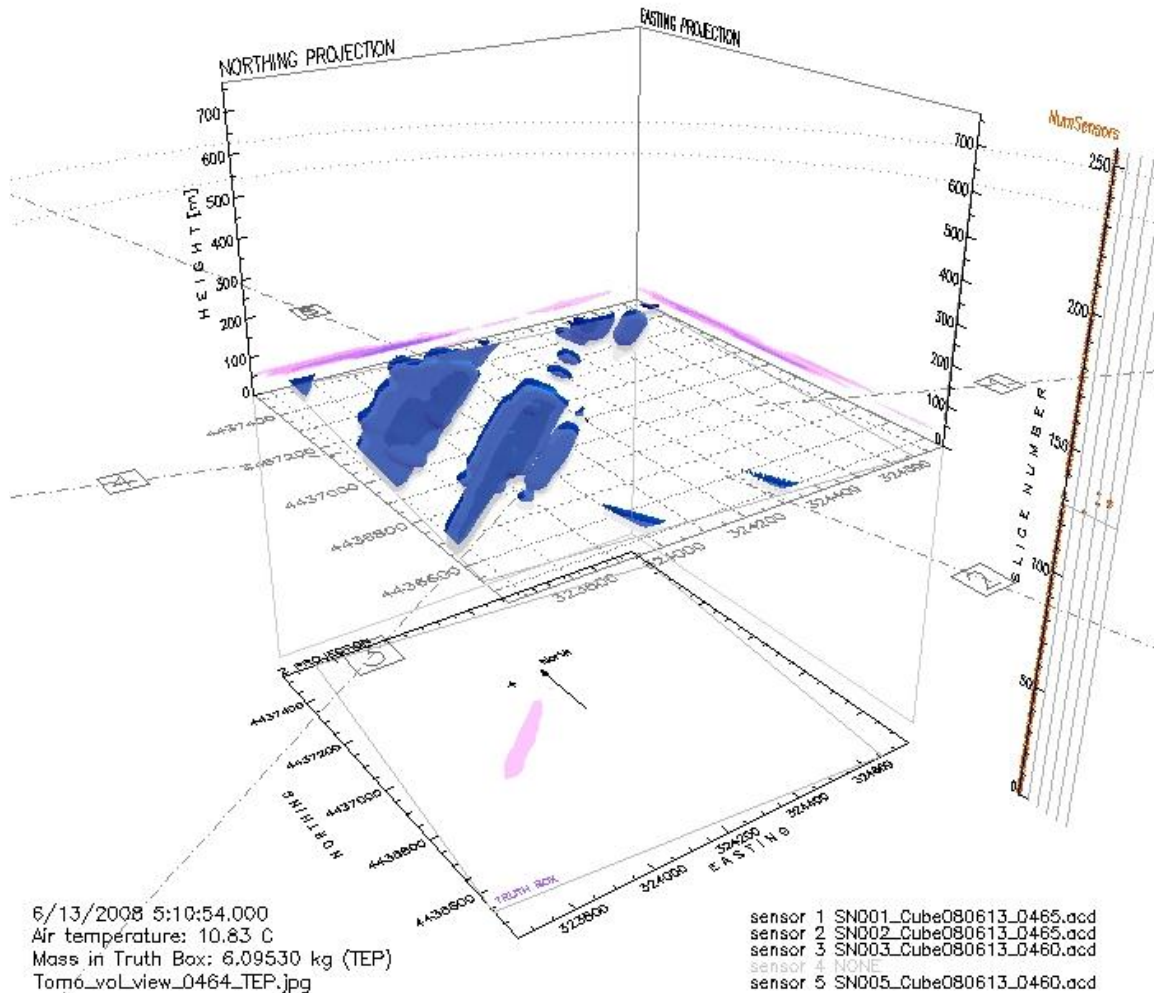
Figure 25. AIRIS voxels from tomographic reconstruction at ground level.

Tables 3, 4, 5, and 6 are examples of the columnar analysis for the 2008 Target-S tests. Table 3 was an explosive release of 150 kg TEP simulant (test #05TE150), and Table 4 was an explosive release of 30 kg of TEP (test #06TE030). Table 5 was an explosive release of 150 kg of TEP (test #09TE150), and Table 6 was a stack release of 30 kg of TEP (test #10TE030). In these tables, column data is turned on its side. That is, the tables list by row the concentration data in lines (really, columns) rising up vertically from the locations of the LCD detectors. (The locations of the LCD detectors according to Figure 7 are provided in the first column of the table.) The concentration values are in units of mg/m^3 and represent a summation over all time steps for which data were available for that test. The number of time steps is constant for all AIRIS data and is provided in the table header row. The first table column of AIRIS data contains the sums over all voxels (*z*-bins) for each data column (i.e., row in the table). The second AIRIS

38
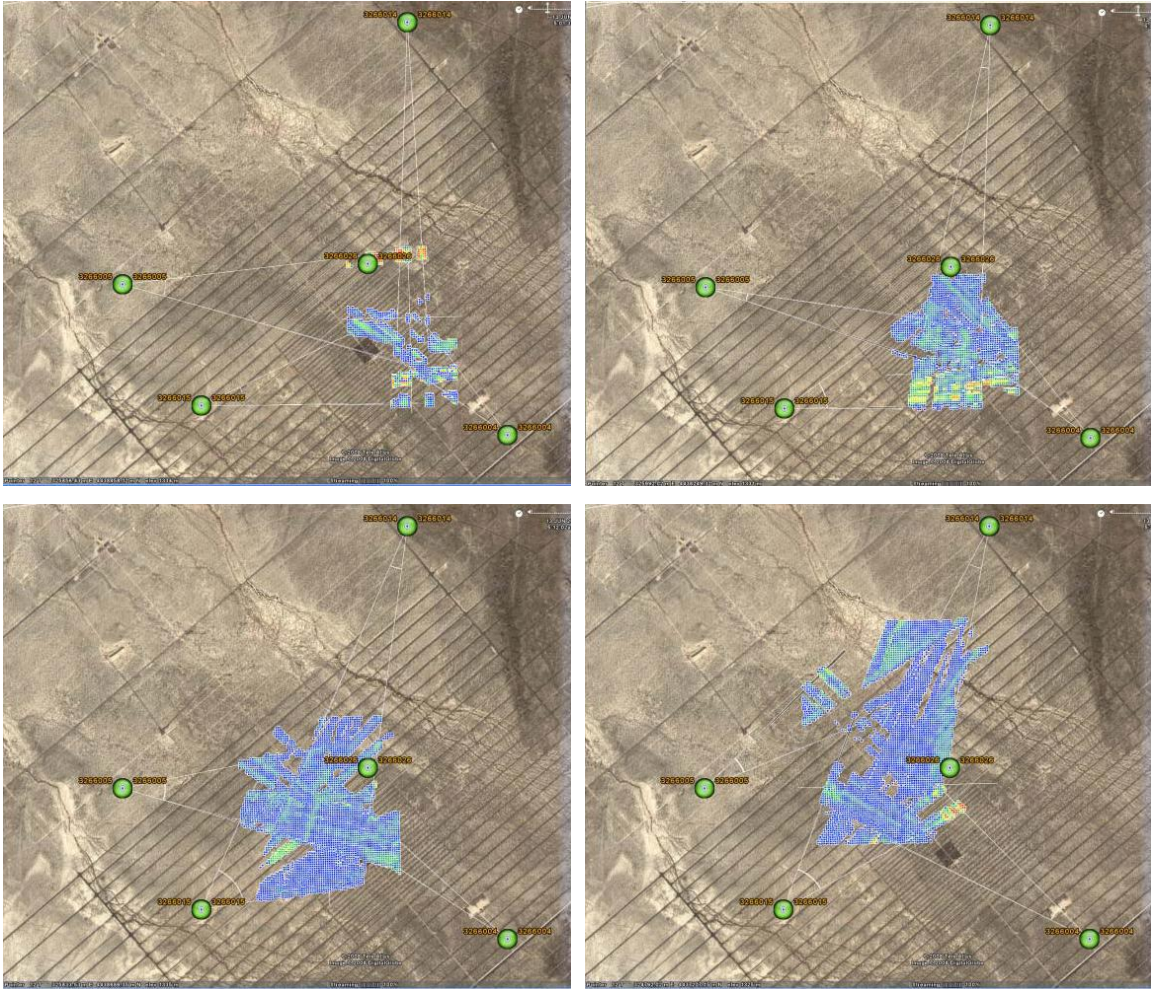
Figure 26. Four different time slices of FTIR data from test #10TE030.

data column, z-bin #128, contains the concentrations of the ground level voxels. Each subsequent z-bin column increases in height by 6 m. Total values of the concentrations for all locations by height are provided in the bottom row.

Examination of table data shows that there was little coincidence between the LCD detectors and AIRIS sensors. For example, the explosive releases in Tables 3 and 4 have very little data from the AIRIS sensors for any height. Even when those data are consistent between sensors, as at location SE in Table 3, the connectivity is awry. Here, the largest concentrations seen by AIRIS are in the two z-bins (#129 and #130) above ground level (z-bin #128) while the ground level concentration (z-bin #128) disagrees significantly with that measured by the LCD detector. A similar pattern is seen in Table 4. Better coincidence between the sensors is seen in Table 5. With the stack release of Table 6, more simulant was released much higher above ground and consequently the AIRIS data track the simulant cloud much more consistently. However, there is still a large disagreement between the LCD and AIRIS systems at ground level, particularly in Table 6. These relationships between the sensors persist even if the concentration values are rounded to the nearest order of magnitude in order to roughly approximate the difference in integration times, a factor which was not considered in these tables.

Table 3. Columnar analysis for Test #05TE150

| Location | LCD Concentraions | | AIRIS Concentrations at Various Z-Bins (98 timesteps) | | | | | | |
	Values	Timesteps	All Z Bins	Z#128	Z#129	Z#130	Z#131	Z#132	Z#133
NW Corner	1526.63	1431	0.00	0.00	0.00	0.00	0.00	0.00	0.00
N Edge	280.29	1647	0.00	0.00	0.00	0.00	0.00	0.00	0.00
NE Corner	79.44	1549	0.47	0.00	0.00	0.00	0.00	0.00	0.00
W Edge	43.41	1667	0.00	0.00	0.00	0.00	0.00	0.00	0.00
Center	12.03	1593	0.00	0.00	0.00	0.00	0.00	0.00	0.00
E Edge	240.46	1650	0.00	0.00	0.00	0.00	0.00	0.00	0.00
SW Corner	2.53	1690	0.00	0.00	0.00	0.00	0.00	0.00	0.00
S Edge	0.00	0	0.00	0.00	0.00	0.00	0.00	0.00	0.00
SE Corner	58.34	1596	23.34	0.48	10.29	12.57	0.00	0.00	0.00
NW1	1213.63	1630	0.00	0.00	0.00	0.00	0.00	0.00	0.00
NW2	0.00	0	0.00	0.00	0.00	0.00	0.00	0.00	0.00
NW3	745.74	1599	0.00	0.00	0.00	0.00	0.00	0.00	0.00
NW4	296.11	1537	0.00	0.00	0.00	0.00	0.00	0.00	0.00
NE1	96.34	1622	1.82	0.00	0.00	0.47	1.34	0.00	0.00
NE2	1028.40	1548	0.00	0.00	0.00	0.00	0.00	0.00	0.00
NE3	11.69	1668	1.32	0.00	0.00	1.32	0.00	0.00	0.00
NE4	706.56	1442	0.00	0.00	0.00	0.00	0.00	0.00	0.00
SW1	2.57	1696	0.00	0.00	0.00	0.00	0.00	0.00	0.00
SW2	0.00	0	0.00	0.00	0.00	0.00	0.00	0.00	0.00
SW3	22.28	1663	0.00	0.00	0.00	0.00	0.00	0.00	0.00
SW4	32.29	1631	0.00	0.00	0.00	0.00	0.00	0.00	0.00
SE1	1.06	1693	0.11	0.00	0.00	0.11	0.00	0.00	0.00
SE2	0.00	0	3.39	0.00	3.08	0.31	0.00	0.00	0.00
SE3	0.00	0	0.04	0.00	0.02	0.02	0.00	0.00	0.00
SE4	77.21	1687	3.57	0.00	3.56	0.00	0.01	0.00	0.00
Totals	6477.02		34.06	0.48	16.96	14.80	1.35	0.00	0.00

Table 4. Columnar analysis for Test #06TE030

LCD Concentrations			*AIRIS Concentrations at Various Z-Bins (157 timesteps)*										
Location	*Values*	*Timesteps*	*All Z Bins*	*Z#128*	*Z#129*	*Z#130*	*Z#131*	*Z#132*	*Z#133*	*Z#134*	*Z#135*	*Z#136*	*Z#137*
NW C	0.00	0	0.00	0.00	0.00	0.00	0.00	0.00	0.00	0.00	0.00	0.00	0.00
N Edge	35.18	83	1.26	1.24	0.01	0.00	0.00	0.00	0.00	0.00	0.00	0.00	0.00
NE C	59.69	143	11.42	11.19	0.23	0.00	0.00	0.00	0.00	0.00	0.00	0.00	0.00
W Edge	0.00	0	0.00	0.00	0.00	0.00	0.00	0.00	0.00	0.00	0.00	0.00	0.00
Center	0.00	0	0.57	0.00	0.00	0.01	0.00	0.00	0.00	0.00	0.00	0.56	0.00
E Edge	299.91	181	26.27	11.93	9.16	5.18	0.00	0.00	0.00	0.00	0.00	0.00	0.00
SW C	1.39	23	0.01	0.00	0.00	0.00	0.00	0.00	0.00	0.00	0.00	0.00	0.00
S Edge	1.79	29	0.03	0.00	0.00	0.03	0.00	0.00	0.00	0.00	0.00	0.00	0.00
SE C	0.00	0	7.18	1.31	0.61	0.69	4.57	0.01	0.00	0.00	0.00	0.00	0.00
NW1	8.82	19	0.02	0.00	0.00	0.02	0.00	0.00	0.00	0.00	0.00	0.00	0.00
NW2	26.16	80	0.00	0.00	0.00	0.00	0.00	0.00	0.00	0.00	0.00	0.00	0.00
NW3	42.05	116	0.00	0.00	0.00	0.00	0.00	0.00	0.00	0.00	0.00	0.00	0.00
NW4	190.29	204	0.58	0.04	0.00	0.54	0.00	0.00	0.00	0.00	0.00	0.00	0.00
NE1	6.75	111	0.12	0.11	0.00	0.00	0.00	0.00	0.00	0.00	0.00	0.00	0.00
NE2	4.34	125	0.38	0.34	0.04	0.00	0.00	0.00	0.00	0.00	0.00	0.00	0.00
NE3	1.64	85	3.00	2.10	0.00	0.89	0.00	0.00	0.00	0.00	0.00	0.00	0.00
NE4	8.17	43	14.82	0.58	14.22	0.03	0.00	0.00	0.00	0.00	0.00	0.00	0.00
SW1	13.41	213	0.01	0.00	0.00	0.00	0.00	0.00	0.00	0.00	0.00	0.00	0.00
SW2	0.00	0	0.01	0.00	0.00	0.00	0.00	0.00	0.00	0.00	0.00	0.00	0.00
SW3	19.27	67	0.00	0.00	0.00	0.00	0.00	0.00	0.00	0.00	0.00	0.00	0.00
SW4	172.91	215	0.00	0.00	0.00	0.00	0.00	0.00	0.00	0.00	0.00	0.00	0.00
SE1	0.00	0	0.06	0.01	0.00	0.03	0.01	0.00	0.00	0.00	0.00	0.01	0.00
SE2	0.00	0	3.01	1.59	0.40	1.00	0.00	0.01	0.00	0.00	0.00	0.00	0.00
SE3	0.00	0	1.58	0.78	0.60	0.19	0.00	0.00	0.00	0.00	0.00	0.00	0.00
SE4	2.29	88	37.91	15.48	14.61	4.38	3.44	0.00	0.00	0.00	0.00	0.00	0.00
Totals	894.08		108.24	46.70	39.89	12.98	8.04	0.02	0.00	0.00	0.00	0.58	0.02

Table 5. Columnar analysis for Test #09TE150

LCD Concentrations			*AIRIS Concentrations at Various Z-Bins (107 timesteps)*										
Location	*Values*	*Timesteps*	*All Z Bins*	*Z#128*	*Z#129*	*Z#130*	*Z#131*	*Z#132*	*Z#133*	*Z#134*	*Z#135*	*Z#136*	*Z#137*
NW C	52.63	1081	36.44	0.00	0.00	0.00	1.96	24.98	9.11	0.39	0.00	0.00	0.00
N Edge	66.00	1158	0.02	0.00	0.00	0.00	0.00	0.01	0.00	0.00	0.00	0.00	0.00
NE C	11.65	1226	0.07	0.00	0.00	0.00	0.00	0.01	0.00	0.00	0.00	0.00	0.04
W Edge	250.83	970	25.08	3.96	3.08	13.36	4.69	0.00	0.00	0.00	0.00	0.00	0.00
Center	55.80	1199	47.04	0.01	1.44	0.00	0.00	0.00	0.02	0.09	0.00	8.66	11.19
E Edge	5.46	1260	0.32	0.00	0.00	0.00	0.00	0.00	0.31	0.01	0.00	0.00	0.00
SW C	13.82	992	0.06	0.00	0.00	0.00	0.00	0.00	0.00	0.00	0.00	0.00	0.04
S Edge	12.32	1114	25.20	0.07	2.95	3.64	13.89	2.71	1.95	0.00	0.00	0.00	0.00
SE C	1102.39	1200	80.90	0.26	7.70	15.38	28.94	28.60	0.01	0.00	0.00	0.00	0.00
NW1	0.00	0	0.01	0.00	0.00	0.00	0.00	0.00	0.00	0.00	0.00	0.00	0.00
NW2	0.00	0	0.07	0.00	0.00	0.00	0.00	0.00	0.07	0.00	0.00	0.00	0.00
NW3	41.80	1131	4.62	0.02	1.74	2.78	0.00	0.00	0.00	0.06	0.00	0.00	0.00
NW4	23.59	1267	0.00	0.00	0.00	0.00	0.00	0.00	0.00	0.00	0.00	0.00	0.00
NE1	118.66	850	0.05	0.02	0.00	0.00	0.00	0.00	0.00	0.01	0.00	0.00	0.02
NE2	4.95	1200	0.03	0.00	0.00	0.00	0.00	0.00	0.00	0.00	0.00	0.00	0.02
NE3	132.07	1030	0.00	0.00	0.00	0.00	0.00	0.00	0.00	0.00	0.00	0.00	0.00
NE4	7.94	1264	0.00	0.00	0.00	0.00	0.00	0.00	0.00	0.00	0.00	0.00	0.00
SW1	223.09	1202	27.85	0.00	17.01	8.48	2.32	0.00	0.00	0.00	0.03	0.00	0.01
SW2	67.18	1118	24.81	5.84	5.48	6.68	6.77	0.00	0.00	0.00	0.02	0.00	0.01
SW3	438.86	1192	15.97	0.00	5.64	4.69	5.64	0.00	0.00	0.00	0.00	0.00	0.00
SW4	92.88	1081	88.65	11.99	17.68	38.44	20.01	0.53	0.00	0.00	0.00	0.00	0.00
SE1	0.00	0	18.22	0.03	6.11	1.03	0.43	3.13	6.08	1.42	0.00	0.00	0.00
SE2	0.00	0	2.29	0.16	0.00	0.00	0.09	1.62	0.23	0.17	0.00	0.00	0.00
SE3	0.00	0	76.03	22.50	14.15	21.01	7.79	9.26	1.31	0.02	0.00	0.00	0.00
SE4	192.70	1234	51.05	0.00	0.01	0.00	0.00	22.55	16.18	12.32	0.00	0.00	0.00
Totals	2914.62		524.79	44.87	82.99	115.48	92.53	93.42	35.27	14.48	0.07	8.67	11.33

42

Table 6. Columnar analysis for Test #10TE030

LCD Concentrations			*AIRIS Concentrations at Various Z-Bins (193 timesteps)*										
Location	*Values*	*Timesteps*	*All Z Bins*	*Z#128*	*Z#129*	*Z#130*	*Z#131*	*Z#132*	*Z#133*	*Z#134*	*Z#135*	*Z#136*	*Z#137*
NW C	31.44	408	76.35	0.00	0.00	1.13	0.00	0.02	0.04	0.06	6.89	37.88	19.68
N Edge	0.00	0	60.06	0.00	0.00	45.24	1.14	1.35	0.00	0.00	1.47	5.57	2.37
NE C	0.14	407	96.94	0.00	0.01	0.00	0.00	0.00	0.00	0.00	0.69	37.46	34.53
W Edge	18.98	597	12.85	0.00	0.00	0.07	0.00	0.04	0.06	0.16	0.00	0.65	3.01
Centrr	8.02	503	299.17	0.00	0.00	1.77	0.25	0.07	0.00	2.02	17.17	170.05	94.15
E Edge	0.16	408	1.56	0.00	0.01	0.00	0.00	0.00	0.00	0.05	0.33	0.09	0.02
SW C	0.90	454	21.55	0.00	0.00	0.01	0.00	0.00	0.00	0.02	1.80	0.35	6.25
S Edge	3.02	409	40.44	0.00	0.00	0.09	0.05	0.00	0.03	16.59	20.02	2.54	0.95
SE C	167.11	696	259.84	0.00	11.84	123.25	37.36	0.15	0.00	0.29	9.06	54.90	21.38
NW1	0.54	536	31.10	0.00	0.00	0.07	0.00	0.02	0.04	0.08	0.17	4.03	5.17
NW2	0.00	0	23.47	0.00	0.00	3.81	0.04	0.00	0.01	0.02	2.49	9.03	7.14
NW3	0.00	0	80.49	0.00	0.00	0.32	7.30	0.00	0.03	0.01	2.69	16.50	37.59
NW4	1.30	364	70.97	0.00	0.01	1.01	19.45	0.06	0.02	2.26	16.09	14.18	11.13
NE1	7.39	412	56.56	0.00	0.00	0.62	1.25	0.14	0.00	0.01	23.74	4.57	5.87
NE2	14.48	433	91.81	0.00	0.00	0.01	0.53	0.00	0.00	5.80	10.87	23.97	22.99
NE3	6.67	421	19.77	0.00	0.00	0.11	1.92	0.15	0.00	0.03	0.03	0.80	14.24
NE4	0.00	0	25.65	0.00	0.01	0.00	0.00	0.00	0.00	0.32	0.12	1.56	19.15
SW1	2.97	471	425.36	0.00	0.00	0.01	0.00	0.02	0.98	44.19	161.68	135.91	30.94
SW2	13.18	588	523.27	0.00	0.00	0.09	0.01	0.02	0.04	7.03	277.02	120.66	73.97
SW3	10.24	561	10.37	0.00	0.00	0.01	0.00	0.05	0.06	0.09	4.46	1.49	4.17
SW4	88.33	698	44.21	0.00	0.00	0.15	0.04	0.00	0.03	1.04	4.57	1.00	36.71
SE1	3.98	411	15.42	0.00	0.00	0.42	0.31	0.08	0.00	6.48	6.72	0.48	0.10
SE2	0.00	0	4.42	0.00	0.00	0.55	1.45	0.15	0.00	0.00	0.28	0.06	0.22
SE3	0.00	0	43.51	0.00	0.00	2.71	9.42	4.86	0.00	11.71	11.45	2.69	0.12
SE4	1.24	380	10.33	0.00	0.01	0.06	2.47	6.34	0.00	0.20	0.08	0.11	0.06
Totals	380.07		2345.48	0.00	11.90	181.51	83.00	13.52	1.34	98.46	579.91	646.53	451.91

The discrepancy of sensors at ground level could be further investigated with the Dugway ppbRAE detectors. These detectors were collocated with the LCD systems to within a distance of a few meters. At each location, one ppbRAE detector was placed 1 m above ground, the same height as the LCD detectors, while the other was placed at a height of 6 m, which placed it on boundary between the first and second AIRIS voxels (z-bin #128 and z-bin #129). Figure 27 shows the response of the ppbRAE detectors during test #05TE150, the same test as that of Table 3. In the figure, the response of the upper detector is shown in blue, the lower in green. With the exception of the NW corner location (NWC), the upper and lower ppbRAE detectors exhibited no coincident detections with collocated detectors at different heights, which confirms the results for Tables 3 - 6 for collocated LCD and AIRIS data. Further, the ppbRAE detections were generally not consistent with those of Table 3. These results were typical for the ppbRAE data; see, for example, Figure 23.
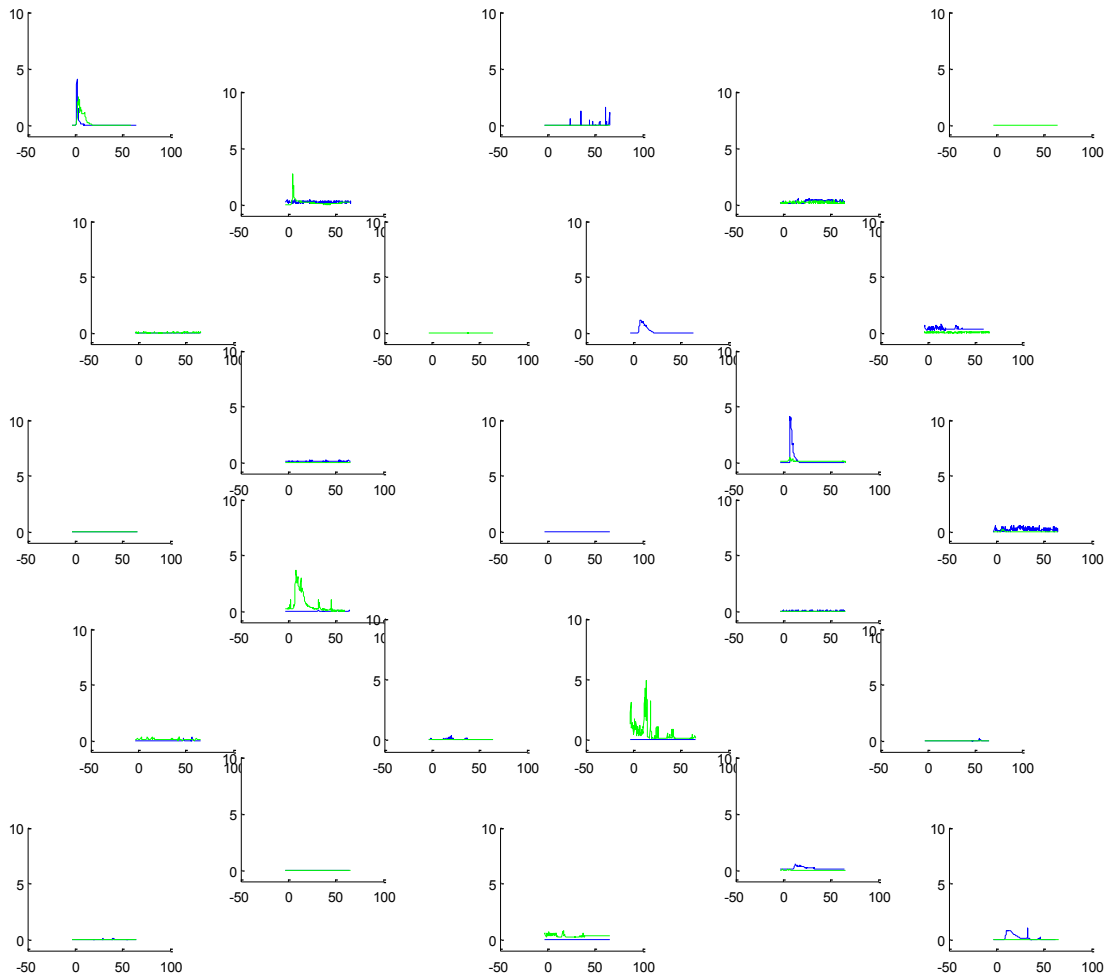
Figure 27. Response of ppbRAE detectors to triethyl phosphate in test #05TE150. The upper ppbRAE detector is in blue, the lower in green.

44

Planar analysis provided further insight into the impact of the method of dissemination for data quality. For the planar analysis, a two-dimensional interpolation algorithm [15] was used to interpolate the LCD data onto a grid of pixels matching the AIRIS voxels at the ground-level plane of the test grid. Interpolation of the LCD data was not ideal, as the data points were sparsely distributed across the grid with distances of 200 m to 300 m between data points. The effect of the 2D interpolation was to distribute the point detections across a larger area surrounding each LCD location and show links between nearest neighbor detectors that could better delineate the extent of the simulant cloud. Because of the sparsity of the LCD data, due partly to few detections and partly to signal variance, the movement of the simulant cloud across the test grid was even less clear than with the standoff data. Further, there was a little agreement between the ground-level AIRIS data and the interpolated LCD data, though this was expected given the results of the columnar analysis. The interpolated LCD data did illuminate some characteristics of explosive and stack dissemination methods. The data indicated that the LCD detectors were seeing simulant that was coming off of the ground, which had been suspected earlier. Ground-reflected simulant was likely due to uneven globular dissemination and evaporation of simulant during an explosive release. Simulant material being reflected off the ground can also explain the lack of concentration detected by the AIRIS sensors for explosive releases.

Finally, in addition to the temperature effects discussed earlier, variations in the wind directions and magnitudes across the test grid were an important factor affecting how the simulant cloud moved across the grid. Measurements of wind speeds and directions were compiled from the Airmar weather stations collocated with the LCD detectors. These results were compiled into a number of movies that simultaneously showed the winds from each station. Compilation movies revealed that even when the winds were flowing steadily in one direction over the test grid there was significant individual variation from this flow over short time scales at every location. Examination of wind data from the PWIDS stations, which continuously gathered data, showed that wind variations were larger during the day than the night. Night testing thus mitigated the wind effect on the testing, but the winds remained a significant source for variation between point sensors at the ground level and for regions monitored by the standoff sensors.

Thus, environmental factors and the dissemination methods both had significant effects on data quality. Wind variations further aggravated uneven, globular dissemination and evaporation of simulant from explosive releases, and disrupted the generation of a smooth plume of simulant from stack releases. It is likely that the variations observed in the LCD data are due largely to these two factors. It is also likely that these factors contributed to the artifact problem observed in the standoff sensor data.

5.3.3 *Improving Data Quality*

A number of techniques may be employed to improve the quality of the RTVS data. For instance, the LCD dropouts are easy to identify and repair retrospectively and were corrected as part of the data fusion analysis. A dropout was identified as a zero-valued data point for which the preceding and subsequent data points were above a small, non-zero threshold. The zero-valued point was replaced with a value interpolated from several nearest neighbor data points. Figure 24 (top) shows an example of LCD data

(blue dots) with two dropouts. The 10-second time intervals are shown in the green vertical lines. Figure 24 (bottom) displays the corrected and interpolated LCD data. The correction was performed simultaneously with interpolation of the LCD data to the 10-second time resolution.

In real time, dropouts are more challenging to identify and correct because of the difficulty in distinguishing a dropout from a legitimate, zero-valued data point without knowledge of the subsequent (i.e., future) data values. Therefore, a real-time correction necessarily requires interpolating over a buffer of the most recent data points and consequently delays further upstream processing of the data by several seconds. For example, a buffer containing the ten most recent LCD data points would incur a delay of 20 seconds for situational awareness, given a 2-second data acquisition rate.

Similarly, the variance observed in the LCD concentration profiles is easily rectified with the use of a moving average filter or interpolation algorithm. The bias-variance tradeoff is a significant challenge when reducing variance; care needs to be taken not to bias the data by over smoothing with a filter. Implementing a filter for real-time processing is also likely to incur a buffer delay for situational awareness.

Decreasing the variance observed in the AIRIS voxels is a more difficult problem. An averaging or interpolating filter, in time, space, or both simultaneously, may lessen the number of artifacts, improve the smoothness, and reduce gaps in the detected cloud, but will almost surely aggravate the intermittent data points appearing sporadically in the data cube by enhancing both the spatial and temporal extents of these artifacts. Rather than averaging, an approach that favors adjacent (nearest neighbor) data points in space and persistent data points in time would be more effective at reducing intermittent data points and reducing gaps.

Another approach to decreasing the variance in AIRIS data is to consider the source of the artifacts, the tomographic reconstruction algorithms. For instance, concentrations detected in the 2D pixel data are mapped to sets of voxels in the 3D reconstructed data. If the mapped data cannot be localized to an individual voxel, then its concentration should be divided equally among all possible voxels that form solutions to the tomographic equations for this 2D data. A Bayesian approach could refine this equipartition of the concentration based on adjacency and persistence requirements. Uncertainties could be estimated from the contributions and partitions of multiple pixels. Such Bayesian values and uncertainties are well suited to pattern recognition and signal processing algorithms.

Binning is another approach appropriate for mitigating the effects of the widely varying concentrations seen in the AIRIS data. For example, reducing the concentrations to one of four possible values (e.g., none, low, medium, high) makes it much easier to identify which voxels are most significant for situational awareness. The boundaries of the four bins can be suitably chosen from a histogram of the concentrations observed in the AIRIS data over a variety of tests. Further, binning does not reduce the effectiveness of the

aforementioned variance reducing approaches and may make their implementation less difficult.

In all of these approaches, the difference between a raw data value and one that has been filtered or modified may serve as a measure of the potential uncertainty in that data value. Such uncertainty estimates can be very effective for multisensor data fusion.

5.3.4 Data Fusion

The discussion of sources of variance in the datasets leads naturally to the development of a frame of discernment appropriate for RTVS data fusion. First, the detections of TEP and MeS simulants by the LCD point sensors were likely to be correct detections with very few false positives. Values for the detected concentrations of simulants were also reasonable. The absence of detections by an LCD point sensor, however, was not a clear indication of the absence of simulant when simulant had been recently detected by the sensor, or detected by an adjacent sensor. Varying wind conditions and data dropouts were both significant sources of false negatives for the LCD sensors.

For the AIRIS data, detections of simulants were likely to be correct indications that simulants were present somewhere in the field of view of the sensors. The precise location was uncertain due to tomographic reconstruction with varying data sources, as were the detected concentration values. The absence of detections was only likely to be correct in the AIRIS data if no detections were observed anywhere in the sensors" fields of view. Thus, the AIRIS sensors were effective at determining whether a simulant was present, but not as effective at determining where the simulant was located at any given time.

The coverage areas of the LCD and AIRIS sensors are effectively disparate and do not overlap. Though the ground-level boundary of the AIRIS coverage area does include the point sensors, boundary effects in the tomographic reconstruction appear to limit the effectiveness of AIRIS at ground level. The lack of overlapping coverage from the LCD and AIRIS sensors limits the performance gains possible with multisensor data fusion.

Together, the LCD and AIRIS sensors form a frame of discernment in which detections of simulants are clear indications of a tangible chemical threat, and the absence of detections is an accurate all-clear signal on the test grid. However, the combined sensors are not able to effectively distinguish local regions of threat from regions of all clear on the test grid when a simulant has been released.

This frame of discernment has implications for the selection of suitable data fusion algorithms. The presence of significant numbers of false negatives means that a Dempster-Shafer approach would be the most effective strategy for RTVS data fusion, as this approach treats all types of information as adding to the total situational awareness, but remains flexible when the absence of information is uncertain or not informative for situational awareness. In addition, heuristic methods would be effective for implementing the algorithms discussed for improving RTVS data quality. Heuristic rules are also likely to be useful for RTVS data fusion as well.

As for the other data fusion methods discussed, a Bayesian approach treats the absence of information with the same significance for situational awareness as the presence of information, and is therefore not well suited for RTVS. False negatives also greatly restrict the selection of potential pattern recognition approaches for RTVS data fusion, as most algorithms treat information in the same manner as the Bayesian approach. Pattern recognition may be effective at improving the number and types of artifacts observed in the standoff sensor data.

6. CONCLUSIONS

- Environmental factors significantly affect the testing at Dugway Proving Grounds. Winds induced significant variance in the RTVS data. Testing at night when winds were less variable mitigated wind effects. An inverted temperature gradient with respect to height may have affected the calibration and sensing capabilities of the standoff sensors. Testing at night increased the effect, as the temperature gradient was positive and less steep during the day.
- A large variation in the RTVS data was observed with respect to the dissemination method. Explosive dissemination generated an uneven, globular release of simulant with unpredictable vaporization. Dissemination by stack release produced a more even distribution of vaporization simulant, but was not consistent with the expected chemical threat scenario.
- The effective calibration and baselines of the LCD point sensors make them a better choice than the Dugway ppbRAE point sensors for RTVS.
- The three-dimensional AIRIS data cube with individual voxels covering the test grid to a great height is an extremely flexible format for data fusion. The problems observed with the tomographic reconstruction will lessen with further experience and computational power.
- Overall, the AIRIS sensors provided cloud-tracking capabilities that were similar to the Dugway MESH FTIR sensors, but were at three-times better resolution. Cloud tracking with either AIRIS or MESH was a vast improvement over tracking with the ORION IR cameras, which typically lost track of the cloud within two minutes of its dissemination.
- The coverage areas of the LCD and AIRIS sensors are effectively disparate and do not overlap, which limits the performance gains possible with multisensor data fusion.
- Together, the LCD and AIRIS sensors provide situational awareness in which detections of simulants are clear indications of a tangible chemical threat, and the absence of detections is an accurate all-clear signal for the test grid as a whole. The combined sensors are not able to effectively distinguish local regions of threat from regions of all clear on the test grid when a simulant has been released.
- The presence of significant numbers of false negatives means that a Dempster-Shafer approach is the most effective strategy for RTVS data fusion. Dempster-Shafer treats all types of information as adding to the total situational awareness, but remains flexible when the absence of information is uncertain or not informative for situational awareness.

- Heuristic methods would be effective for implementing the algorithms discussed for improving RTVS data quality. Heuristic rules are also likely to be useful for RTVS data fusion.
- Real-time situational awareness is possible from fused LCD and AIRIS data, but the rate is limited to at best one update per minute covering the whole test grid. The performance will improve with increased computational power and better reconstruction algorithms.

7. ACKNOWLEDGEMENTS

8. REFERENCES

[1] S. Rose-Pehrsson, K. Johnson, C. Minor, V. Guthrie, "Final Report: Intelligent Data Fusion for Wide-Area Assessment of UXO Contamination", SERDP Project MM-1510, Naval Research Laboratory, 31 Jan 2008. http://docs.serdp-estcp.org/

[2] H. Davila, "Test Record for Range Test Validation System (RTVS) 07, Test Project number 2007-DT-DPG-ARSPT-D6060", Department of the Army, US Army Dugway Proving Ground, Dugway, UT 84022-5000, WDTC-RR-07-117, Dec. 4, 2007.

[3] H. Davila, G. Bowers-Irons, "Final Test Report for the Range Test Validation System 2008 (RTVS-08), ATEC Project No. 2008-DT-DPG-NBCDT-D8626", West Desert Test Center, US Army Dugway Proving Ground, Dugway, UT 84022-5000, WDTC-TR-08-060, Oct. 7, 2008.

[4] D. L. Hall and A. K. Garga, "Pitfalls in Data Fusion (and How to Avoid Them)", Proc. 2nd Internat. Conf. Information Fusion, vol. 1, pp. 429-436, 1999.

[5] L. A. Klein, *Sensor and Data Fusion: A Tool for Information Assessment and Decision Making*, SPIE Press, Bellingham, WA, 2004.

[6] R. O. Duda, P. E. Hart, and D. G. Stork, *Pattern Classification.* New York, John Wiley & Sons, Inc., 2001.

[7] S. James Press, *Bayesian Statistics: Principles, Models, and Applications*, John Wiley & Sons, New York, 1989.

[8] D. S. Sivia, *Data Analysis: A Bayesian Tutorial*, Oxford University Press Inc., New York, 1996.

[9] G. Shafer, *A Mathematical Theory of Evidence*, Princeton University Press, Princeton, NJ, 1976.

[10]   Z. Yi, Y. Khing, C. C. Seng, Z. X. Wei, "Multi-ultrasonic sensor fusion for autonomous mobile robots", Proceedings of SPIE, Vol. 4051, 314-321, 2000.

[11]   A. Sarkar, A. Banerjee, N. Banerjee, S. Brahma, B. Kartikeyan, M. Chakraborty, K.L. Majumder, "Landcover classification in MRF context using Dempster-Shafer fusion for multisensor imagery", IEEE transactions on image processing 14(5), 634-45, 2005.

[12]   M. Raza, I. Gondal, D. Green, R. L. Coppel, "Fusion of FNA-cytology and gene-expression data using Dempster-Shafer Theory of evidence to predict breast cancer tumors", Bioinformation 1(5), 170-5, 2006.

[13]   K. Sentz and S. Ferson, "Combination of Evidence in Dempster-Shafer Theory", Sandia National Laboratories Report SAND 2002-0835, April 2002.

[14]   B.R. Cosofret, D. Konno, H. S. Kindle, C. M. Gittins, M. L. Finson, and W. J. Marinelli, "Imaging Sensor Constellation for Tomographic Chemical Cloud Mapping", Physical Sciences Inc., 20 New England Business Center, Andover, MA, USA 01810-1077.

[15]   The MathWorks, Inc., *Using Matlab*, version 6, pps. 12-10 – 12-16. MathWorks, Inc., Natick, MA, 2000.

APPENDIX A

RTVS dissemination logs for the 2007 (Table A1) and 2008 (Table A2) test series.

Table A1. RTVS07 Dissemination Log Data

Trial Name	Date (Sept 2007)	Referee Start Time	Release Time	Trial End Time	Dissemination Area[a]	Dissemination Points[b]	Amount of TEP[b] Disseminated (kg)
01T010	17	13:15:00	13:30:00	13;43:00	NNW	14,15,18,19	10
01T010	18	07:30:00	07:45:00	08:03:00	NNW	14,15,18,19	10
02T010	18	14:14:00	14:30:00	14:36:00	SSE	14,15,18,19,22,23	30
03T030	19	07:45:00	07:57:00	08:25:00	SSW	E13	30
04T030	19	08:55:00	09:08:00	09:34:00	SSW	E13	50
05T030	19	10:03:00	10:18:00	11:02:00	SSW	E13	30
06T100	19	11:02:00	11:45:00	12:20:00	SSW	E13	100
07T050	20	10:58:00	11:18:00	11:39:00	SSE	13,14,15,16,17,18,19,20,22,23	50
08T050	20	12:27:00	12:41:00	12:51:00	SSE	13,14,15,16,17,18,19,20,22,23	50
09T160	20	14:09:00	14:22:00	14:55:00	SSE	16,24	160
10T050	21	06:04:00	07:16:00	07:42:00	SSW	E13 (3 points)	50
11T080	21	08:15:00	08:30:00	09:1500	SSE	23,24	80
12T120	21	09:28:30	09:34:00	10:28:00	SSE	18,19,21,22,23,24	120
13T160	21	10:56:00	11:15:30	11:38:00	SSE	17,18,19,20,21,22,23,24	160

[a]NNW – North Northwest; SSE – South Southeast; SSW – South Southwest.
[b]Triethyl phosphate.

Table A2. RTVS08 Dissemination Log Data

Trial Name	Date (June 2008)	Referee Start Time	Release Time	Trial End Time	Dissemination Location[a]	Detonation Points[b]	Simulant Amount (kg) Planned	Simulant Amount (kg) Actual	Simulant Type[c]	Comment[a]
01TE030	9	0033	00:46:30	01:15:30	S2	A	30	30	TEP	None
02TE030	9	0143	01:53:00	02:14:00	S2	A	30	30	TEP	None
03TE075	9	0404	04:31:00	05:03:00	S2	B	75	75	TEP	None
04TE075	10	0437	04:47:00	05:45:30	S3	B	75	75	TEP	None
05TE150	11	2243	22:53:00	23:58:00	N2	B	150	150	TEP	None
06TE030	9	2316	23:46:15	00:25:00	S3	A	30	30	TEP	None
07TE030	10	0546	05:58:00	06:32:30	S2	A	30	30	TEP	None
08TE075	10	0108	01:23:00	02:09:00	S2	B	75	75	TEP	None
09TE150	10	0241	02:46:00	04:34:00	S2	B	150	150	TEP	None
10TE030	12	2253	22:55:00	23:41:00	WC	NA	30	55.13	TEP	e
11TE075	13	0048	00:49:45	01:37:00	WC	NA	75	78.16	TEP	D
12TE075	13	0137	01:47:00	02:57:00	WC	NA	75	73.77	TEP	E
13TE150	13	0257	03:07:00	04:14:00	WC	NA	150	146.21	TEP	F
14TE075	ND	ND	ND	ND	ND	ND	ND	ND	ND	G
15TE150	12	0233	03:35:00	05:55:30	S2	B	150	150	TEP	None
16TE150	13	0508	05:13:00	07:00:00	S2	B	150	150	TEP	None
17TE150	ND	ND	ND	ND	ND	ND	ND	ND	ND	NA
18MS030	14	0620	06:30:00	06:56:00	S2	A	30	30	MeS	None
19M5030	16	0138	01:43:00	02:07:30	S2	A	30	30	MeS	None
20BL000	14	0032	00:42:00	00:57:00	S2	B	None	None	None	H
21MT030	14	0124	01:40:00	02:46:00	S2	A	30/30	30/30	MeS/TEP	None
22MT075	14	0246	03:17:00	03:43:00	S2	B	75	75	MeS/TEP	None
23MS030	16	0354	03:55:00	05:03:00	S2	A	30	30	MeS	None
24MS075	ND	ND	ND	ND	ND	ND	ND	ND	ND	NA
25MS075	17	0047	00:52:00	01:20:00	S1	B	75	75	MeS	None
26MS150	ND	ND	ND	ND	ND	ND	ND	ND	ND	NA
27MS075	ND	ND	ND	ND	ND	ND	ND	ND	ND	NA
28MS075	ND	ND	ND	ND	ND	ND	ND	ND	ND	NA
29MS150	18	0103	01:11:00	01:50:00	N3	B	150	150	MeS	None
30MS150	18	0351	03:52:00	04:51:00	N2	B	150	150	MeS	None

Trial Name	Date (June 2008)	Referee Start Time	Release Time	Trial End Time	Dissemination Location[a]	Detonation Points[b]	Simulant Amount (kg)		Simulant Type[c]	Comment[a]
							Planned	Actual		
31MS075	ND	ND	ND	ND	ND	ND	ND	ND	ND	NA
32MS150	18	0442	04:55:00	05:17:00	N2	B	150	150	MeS	None
33MS150	ND	ND	ND	ND	ND	ND	ND	ND	ND	NA
34MS150	ND	ND	ND	ND	ND	ND	ND	ND	ND	NA
35AA030	18	2211	22:22:00	22:59:00	N3	A	30	30	AA	None
36AA075	18	2344	23:55:00	00:32:00	N3	B	75	75	AA	None
37AA075	19	0112	01:20:00	01:44:00	N2	B	75	75	AA	None
38AA150	19	0306	03:14:30	04:25:00	N2	B	150	150	AA	None
39AA150	ND	ND	ND	ND	ND	ND	ND	ND	ND	NA

[a]S2 - south second; S3 - south third; WC - west and center; ND - no data; S1 - south first; N3 - north third; N2 - north second.

[b]A - 2, 3, 6, 7, 10, and 11; B - 1 through 12; NA - not available.

[c]TEP - triethyl phosphate; MeS - methyl salicylate; AA - acetic acid.

[d]C - 40 kg west stack over a 10 min period, 15.13 center stack over a 13 min period; D - 37.59 kg west stack over a 15 min period, 40.57 kg center stack over a 15 min period; E - 38.12 kg west stack over a 15 min period, 35.15 kg center stack over a 15 min period; F -71.48 kg west stack over a 16 min period, 74.72 kg center stack over a 16 min period; G - trial canceled by customer; H - no simulants used; only detonation to create dust cloud.